T H E  U N I V E R S I T Y  O F  T U L S A

THE GRADUATE SCHOOL

# OPTIMIZATION OF SAGD OPERATIONS USING DERIVATIVE FREE ALGORITHMS

by
Emil Nurmammadov

A thesis submitted in partial fulfillment of
the requirements for the degree of Master of Science
in the Discipline of Petroleum Engineering

The Graduate School
The University of Tulsa

2011

T H E  U N I V E R S I T Y  O F  T U L S A

THE GRADUATE SCHOOL

# OPTIMIZATION OF SAGD OPERATIONS USING DERIVATIVE FREE ALGORITHMS

by
Emil Nurmammadov

A THESIS

APPROVED FOR THE DISCIPLINE OF

PETROLEUM ENGINEERING

By Thesis Committee

_____, Chair
Gaoming Li

_____
Albert C. Reynolds

_____
Jingyi Chen

ABSTRACT

Emil Nurmammadov (Master of Science in Petroleum Engineering)

Optimization of SAGD Operations using Derivative Free Algorithms

Directed by Gaoming Li

65 pp., Chapter 4: Conclusions

(539 words)

Steam assisted gravity drainage (SAGD) is an effective thermal recovery method for heavy oil and bitumen extraction. The SAGD process involves many parallel pairs of horizontal injectors and producers. The vertical spacing between the horizontal injector and producer within a pair is 5 to 10 m and the horizontal distance between neighbor wellpairs is 100 to 150 m. After the preheating period, in which steam is circulated in both wells to mobilize oil around wells through heat conduction, the upper horizontal well injects steam into the formation and forms a steam chamber. As the injected steam encounters cold heavy oil and bitumen at the boundary of steam chamber, it condenses and the released latent heat mobilizes more oil. The mobilized oil and steam condensate then flow down, due to gravity, to the producer along the edge of steam chamber.

SAGD is a heat intensive recovery method. Its economic success requires an effective heat management program that prevents heat loss during steam transportation through the pipes and wells, heat loss to caprock and base formation, and heat loss due to idle steam circulation between the injectors and producers. The heat loss in pipes

and wells is decreased with by better facility design while the injection and production strategies need to be adjusted to effectively use the injected steam to heat up cold oil inside the reservoir. To reduce heat loss to caprock, one needs to decrease the steam injection rate after the steam chamber reaches caprock so that the steam chamber can grow laterally. In the actual operations, it is impossible to know when the steam chamber has reached caprock. To prevent direct live steam production, it is necessary to maintain a liquid pool around the producer such that the injected steam is diverted up and laterally to contact cold regions of the reservoir. High production rates will dry up the liquid pool and draw the injected steam directly to the producer. In this case, the injected steam will be circulated back to surface without touching any cold oil in the formation. However, if the production rate is too low, then the liquid pool level might rise even above the injector which leaves a smaller contact area between the steam and cold oil.

Steam trap control has been applied in the field to deal with steam production. Using subcool temperature, difference between the injected steam and produced fluids temperatures is monitored and kept above certain specified value by adjusting the production schedule. However, the optimal subcool temperature is usually unknown and even if it is known, it might not be optimal to keep a constant subcool temperature for the entire production life of the reservoir. In addition, the modeling of subcool used in the simulator does not change the injection schedule but the production schedule only, which may result in any sub-optimal solutions.

In this study, the cold water equivalent (CWE) steam injection rate and producer bottomhole pressure are divided into some control steps and are adjusted to maximize the net-present value (NPV) using the simultaneous perturbation stochastic approximation (SPSA) and ensemble-based optimization (EnOpt). Both algorithms achieve higher final NPV than the subcool reactive control with smaller cumulative steam-oil ratio (cSOR), which is consistent with the goal of heat management.

ACKNOWLEDGEMENTS

I owe my deepest gratitude to my thesis advisor Dr. Gaoming Li for his generous support, valuable assistance and continuous guidance. I specially thank Dr. Albert C. Reynolds, who assisted and encouraged me in various ways during the course of my studies. I extend my gratitude to Dr. Jingyi Chen for serving on my thesis committee.

I am thankful to the Computer Modeling Group (CMG) for providing the necessary simulator licenses.

I would like to express my gratitude to all faculty members and staff of the Petroleum Engineering department of The University of Tulsa, especially Judy Teal and Loreta Watkins. I also wish to express my sincere appreciation to the TUPREP students for being wonderful colleagues and friends for the past two years.

This work is dedicated to my parents and my brother for their unconditional love.

TABLE OF CONTENTS

LIST OF TABLES

Page

LIST OF FIGURES

CHAPTER 1

# INTRODUCTION

There are vast deposits of heavy oil and bitumen in the world, which make up about 70% of the total oil resources [3]. Most of the heavy oil reserves (over 90%) are found in Canada and Venezuela [39]. There is a great interest in the oil industry to produce these crudes economically to meet the ever-increasing energy demand in the world. The biggest challenge to produce heavy oil and bitumen is its high viscosity. The regular heavy oil has an API gravity less than 22.3 and viscosity greater than 10 cp and up to $1 \times 10^6$ cp [1, 2] while bitumen is even more viscous and may not be able to flow at the reservoir conditions. Except direct surface mining for some shallow tar sands, all methods to produce heavy oil and bitumen involve some type of thermal process that reduces oil viscosity by introducing heat to the reservoir [4, 14, 39]. The oil viscosity may decrease from millions of centipoise at reservoir temperature to 10-20 centipoise when the reservoir temperature is raised to about 200 °C with steam injection [10]. Some of the widely used thermal recovery techniques are steam flooding and cyclic steam stimulation which have been successfully applied to heavy oil reservoirs in Venezuela and US [39]. For steam flooding, it is required to have good communication between the injectors and producers such that the steam can be injected to push the mobilized oil towards the producer. This type of communication is difficult to achieve for extra-heavy oil and bitumen reservoirs when the injector-producer spacing is relatively large. Another problem with steam flooding in heavy oil reservoirs is that as the oil is displaced away from the steam chamber it cools down with increasing viscosity, hence lower mobility. Therefore, steam flood can only be used in regular heavy oil reservoirs. The cyclic steam stimulation process does not require

interwell communication. Instead it uses the same well for both steam injection and oil production. After steam is injected for a period of several weeks, there is a soak period that allows steam chamber to further expand and mobilize more oil. It is followed by an extended period of oil production. This process is used extensively in California and Venezuela. There is an increasing application to the bitumen production in Canada [11]. However, this process has a relatively low oil recovery of about 15-20% [10] due to a limited chamber size and lack of driving force to move the hot oil to the producer [11]. Usually a regular heavy oil reservoir starts with cyclic steam stimulation and later converts to steam flooding.

The steam assisted gravity drainage (SAGD) process was introduced by Butler et al. [12, 13] in early 1980's. It proves to be an efficient thermal recovery technique for extra heavy oil and bitumen reservoirs with reported recovery over 50% [9, 34, 38, 45].

## 1.1 Literature Review

### *1.1.1 The SAGD Concept*

The conventional SAGD process (Fig. 1.1) consists of many parallel horizontal wellpairs that are 100-150 m from each other [42] and within each pair, the horizontal injector is located right above the horizontal producer and the typical vertical spacing between the two wells in the pair is 5-10 m [38, 45, 48]. The injector and producer have about the same length (about 500-750 m [34]) and are aligned with each other in parallel. Fig. 1.1 shows a cross-section that is perpendicular to the horizontal wells for one pair in the SAGD process. The SAGD process starts with a preheating period which may take several weeks to months [42]. In this period, the steam is injected through the tubing and circulated back to surface through the annulus in both wells. The bitumen around the wells is heated up and becomes mobile oil due to heat conduction from the circulated steam. Once the steam circulation creates a hydraulic connection between two wells, the bottom horizontal well is converted to a producer and the upper

horizontal well becomes a steam injector. Due to gravity force, the injected steam rises up and forms a steam chamber. When the steam encounters the cold reservoir rock and bitumen at the boundary of the steam chamber, it condenses and passes on its latent heat to the surrounding reservoir rock and bitumen. The heated bitumen then becomes mobile as a result of significant decrease in viscosity [12]. Driven by gravity the heated oil and condensed water drain down to the bottom of the reservoir where it is produced through the production well(see Fig. 1.1). As the high temperature oil continues to drain to the bottom of the reservoir, the injected steam rises up and fills the vacated pore spaces, which allows continuous steam injection and growing steam chamber [11]. Usually, the steam chamber grows vertically and reaches the top boundary (caprock) first and then it expands laterally. The SAGD process is terminated when the steam chambers between nearby wellpairs meet. In the SAGD process, once the oil is heated, it remains hot as it drains to the producer because its flowing path is next to the high temperature steam chamber. This makes SAGD applicable to the extra-heavy oil and bitumen reservoirs.

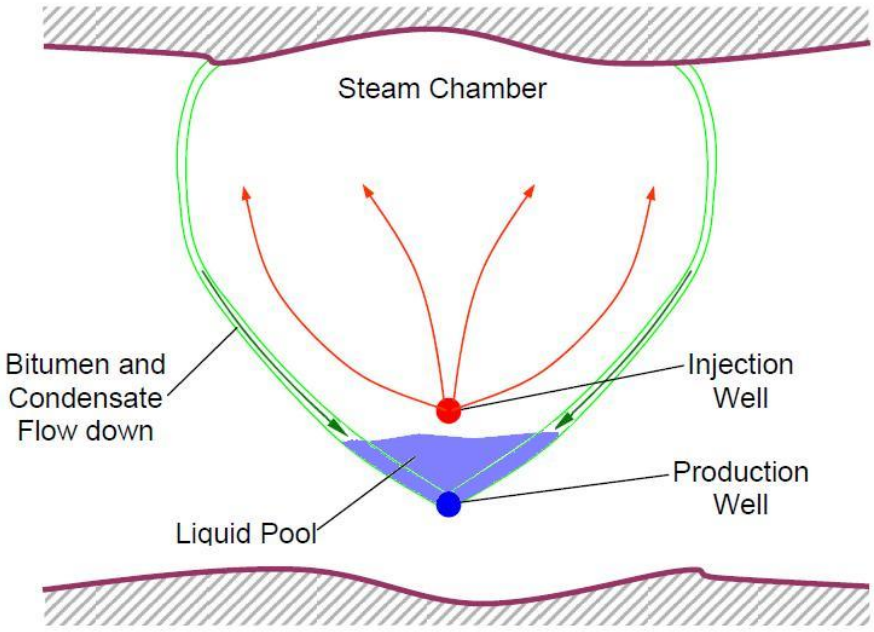


Figure 1.1: The SAGD Concept [29].

Due to high temperature within the steam chamber, most bitumen becomes mobile and is displaced to the producer by the steam. Therefore, the recovery efficiency of the SAGD process relies heavily on the growth of the steam chamber. Note that the replacement of oil by steam within the steam chamber also helps maintain the reservoir pressure and hence the driving force [9]. To have a fast growing steam chamber, one needs to prevent direct steam production and confine the steam within the chamber so that the steam latent heat can be passed on to the bitumen surrounding the chamber when it condenses at the edge of the chamber. The key to make this occur is to maintain a liquid pool around the producer so that the injected steam is diverted away from the producer [30].

Fig. 1.1 shows that the mobilized oil and steam condensate flow down towards the producer at the edge of the steam chamber and they are then produced to surface. When the bottom well produces at high rate, the mobilized oil and steam condensate can soon be depleted and no liquid pool will be formed. If there is no liquid pool, some injected steam will flow down to the producer and then be produced directly without touching any cold bitumen, which hence reduces the energy efficiency of the SAGD process. However, if the production rate is kept too low compared to the steam injection rate, the mobilized oil and steam condensate may accumulate so much that the liquid pool level is even above the injector (Fig. 1.2), which also reduces the steam-cold bitumen contact area and hence steam chamber growth. A second effect for a large accumulation of the mobilized bitumen and steam condensate around the producer is that the temperature around the producer can be cooled down and be much lower than that of the injected steam. As a result, the oil viscosity may significantly increase, which reduces the well productivity.

Maintaining an appropriate level for the liquid pool is called steam trap control in the literature [30]. In order to maintain an appropriate liquid pool level, one needs to monitor and adjust the pressure differential between the injector and producer. As the injected steam is at its saturation state, the pressure and temperature are on the

vapor pressure curve (Fig. 1.3). To maintain a liquid pool around the producer, the pressure and temperature have to be in the liquid region (i.e. to the left of the vapor pressure curve in the pressure-temperature diagram, see Fig. 1.3). Due to the gravity effect, it is possible to have a negative pressure differential between the injector and producer. However, due to its fluctuation behavior, it is not easy to monitor and control the bottomhole pressure of the producer. Instead, people usually use the temperature differential between the injector and producer for steam trap control. This temperature difference between the injected steam and produced fluids is denoted as subcool. Small or zero subcool indicates small or no liquid pool. Large subcool indicates large liquid pool around the producer.

The literature reports that the typical values used in the field practice for the subcool temperature have been between 20 to 40 °C [23, 31]. Even though some studies [6, 28, 29] used subcool as the main producer well constraint, Das [20] argued that subcool temperature does not have significant impact on production under certain conditions due to the complex relationship among the subcool, liquid level, pressure and cumulative injected steam to produced oil ratio (cSOR) [21]. Edmunds [22, 23] mentioned that using subcool as an operating control may not be favorable due to the inaccurate bottomhole temperature measurements for long horizontal wells, and it is recommended to use production rates as the operating constraint.

### *1.1.2 SAGD Optimization*

As the SAGD process is an energy intensive oil recovery method, its economics to a large extent depends on effective heat management, i.e. recover more oil with less steam injection. The aforementioned steam trap control can effectively increase the steam chamber growth and manage the heat usage if the appropriate liquid pool level around the producer is properly maintained. Egermann et al. [24] developed a methodology to optimize the development of steam chamber in the SAGD process for better oil recovery and heat management. In their method, the steam injection rate

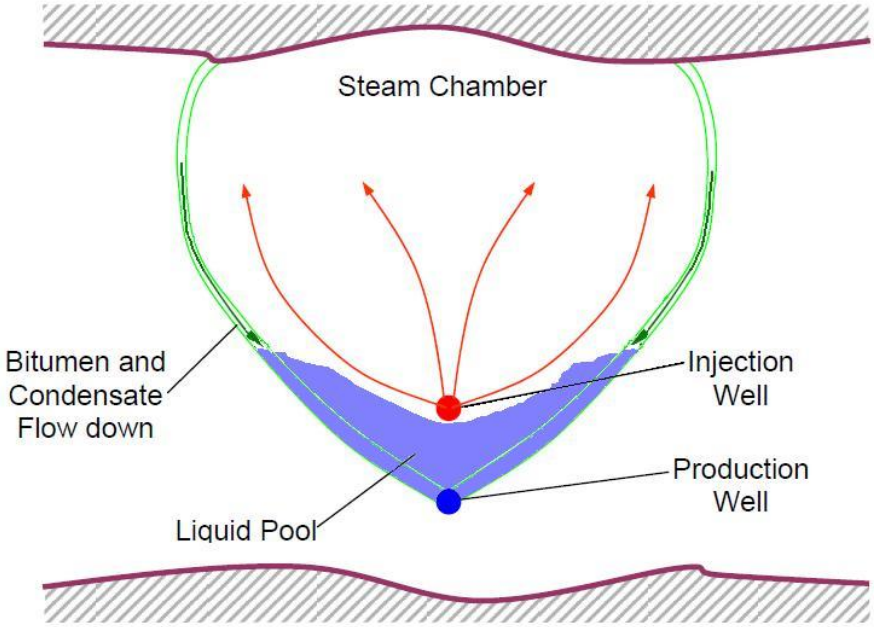


Figure 1.2: Liquid pool above the injector [29].

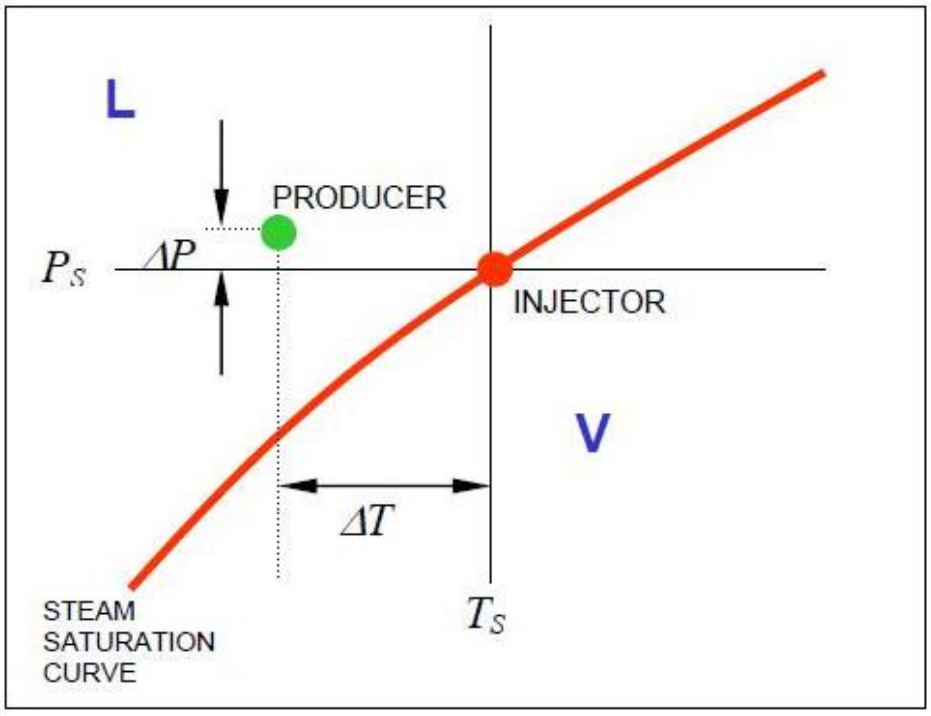


Figure 1.3: Pressure-temperature diagram [29].

is calculated based on the reservoir production potential using the analytical model developed by Butler and Stephens [13] and the oil production rate is adjusted using

the temperature difference between the injected steam and produced fluids, i.e., subcool temperature. The method is applied to a synthetic case and a field case, and the authors argued that it gives optimal results which are in good agreement with Butler's analytical model in terms of oil production rate and the shape of steam chamber. However, the optimal subcool temperature is usually unknown and cannot be easily determined. In addition, due to the formation heterogeneity, the liquid level varies along the horizontal wells and the subcool temperature may exhibit complex behavior, which makes subcool control even more difficult [21]. Most studies on SAGD optimization use cSOR, oil recovery or net-present-value (NPV) as the objective function.

Gates and Chakrabarty [28] applied a genetic algorithm to minimize cSOR by adjusting steam injection stategies. They used injection pressure as the control parameter and the production is controlled using a fixed subcool temperature of 5 °C. Their results show that steam injection pressure should be kept at high values at early times of the SAGD process to allow maximum steam injection and steam chamber growth and injection pressure should be reduced after the steam chamber reaches the top of the reservoir in order to reduce heat loss to the caprock. After minimization, the algorithm was able to reduce cSOR from 35% to 50% for the cases in the paper. They concluded that the genetic algorithm was efficient for SAGD optimization for relatively simple 2D reservoir models, but more efficient algorithms and better computer hardware are needed for complex 3D reservoir models. Gates et al. [29] extended their study to a two-wellpair case in a 3D heterogeneous reservoir with a top gas zone. However, they applied manual production optimization instead of using the genetic algorithm. Due to high computer run time cost, each wellpair is optimized separately to achieve a minimum cSOR using injection pressure as the control and fixed subcool of 5 °C. Similar optimal injection strategies to that in [28] are obtained from each wellpair, i.e., high injection pressure before the steam chamber contacts the top gas zone and subsequently low injection pressure to avoid heat loss to the top gas thief zone. The injection strategies from each wellpair are then combined after individual optimization. Due to

steam chamber communication through the top gas zone, only suboptimal injection strategies can be obtained when the individual wellpairs are optimized separately. Bao et al. [6] also investigated the optimal operating strategies of the SAGD process with a top gas thief zone. They first minimized cSOR using CMG's proprietary DECE (Designed Exploration and Controlled Evolution) optimization algorithm by adjusting injection pressure. The DECE method used in this study consists of two stages: exploring the search space to obtain maximum information about the solution space and improve the given objective function using statistical analysis for the performed simulation runs. However, it is not clear how the production control was set during the injection strategy optimization. The SAGD process is then further improved by adjusting the subcool control along time. The results show that the optimal operating strategies for injection pressure are similar to that in [28, 29] and the variable subcool (high subcool at early time and then a decreasing subcool at late time) can further improve the oil production in the SAGD process. The above papers that use cSOR as the objective function for minimization, show that the optimization can significantly reduce the field cumulative steam injection hence cSOR, however, the cumulative oil production can also be significantly decreased, hence low oil recovery. Another paper that minimizes cSOR is from Card et al. [15]. In this paper, the authors proposed an automated global optimization method by constructing response surface of the cost function, cSOR and the steam injection pressures to optimize the commercial SAGD operations. However, no results were given in the paper.

As the minimization of cSOR is not always consistent with the maximization of oil production, Queipo et al. [43] proposed an objective function that uses a weighted sum of the cumulative oil production and cumulative steam injection. The optimization is done through a surrogate model constructed with neural network. The algorithm is denoted as NEGO (neural network based efficient global optimization). The adjusting parameters during optimization include both the operational controls (injection pressure, injection enthalpy and subcool temperature) and a geometrical design parameter -

vertical injection-production well spacing. Shin and Polikar [48] did a sensitivity study of the operational control parameters (preheating period, steam injection pressure, maximum steam injection rate) and some geometrical parameters (injector-producer well spacing, reservoir thickness) to cSOR, oil recovery factor, oil production rate and NPV.

Although the optimization on the weighted sum of the cumulative oil production and cumulative steam injection considers both the oil recovery and heat management, the weights on the two terms do not have any physical meaning and are arbitrary in nature. A more systematic way is to maximize the net-present value (NPV), which includes three terms: oil production, water production and steam injection and the weights of these terms are the price of oil, cost for produced water treatment and steam generation and transportation per unit volume. Yang et al. [54] maximized NPV for the SAGD process using CMG's proprietary DECE (Designed Exploration and Controlled Evolution) method. The controls for optimization in their paper are steam injection and liquid production rates. Their results show that the NPV maximization is consistent with steam trap control and the final optimal controls resulted in 35% increase in NPV and 30 % decrease in cSOR with fully developed steam chamber. Yang et al. [55] extended their SAGD production optimization to robust optimization, which takes into account of geological uncertainty. Due to geological uncertainty, the optimization based on a single but uncertainty geological model (denoted as nominal optimization) may impose the risk that final optimal controls obtained using this model may not achieve the highest NPV when they are applied to the actual reservoir. In the robust optimization, they used a set of geological models to represent the uncertainty in geology. The objective function they used is the expectation of NPV, which is approximated by the average NPV obtained from the set of geological models. They first generated 100 geological models and obtained the NPVs from each geological model by running the simulator. Then, the NPVs are sorted and ranked from low to high according to their values. Due to high computational cost for simulation runs,

they picked out 9 geological models from the 100 uniformly in the NPV distribution for robust optimization. Their optimization procedure was performed using a second order polynomial proxy model. The well control parameters are maximum bottom-hole pressure for the injection wells and maximum steam production rate for production wells. In the example, the reservoir has both top and bottom water layers, which are heat thief zones. In this case, the well locations will affect the performance of the SAGD process. The injector-producer spacing is fixed to 5 m but their location is subject to optimization in addition to the well control parameters. After robust optimization, the final optimal controls are then applied to the 100 geological models. Compared to the nominal optimization, the final controls from robust optimization yields higher expected NPV and smaller cSOR from the 100 models.

Zhao et al. [56] show that production optimization using the gradient calculated with adjoint method [8, 7, 16, 35, 46, 47] give the fastest convergence with the smallest number of reservoir simulation runs. However, the gradient calculation using adjoint method requires knowledge of the detailed numerics of the reservoir simulator, so the adjoint option is seldom available in commercial reservoir simulators, especially the ones dealing with special EOR processes such as SAGD. This study will test two optimization algorithms that are based on approximate gradients: Simultaneous Perturbation and Stochastic Approximation (SPSA) and Ensemble Based Optimization (EnOpt).

### *1.1.3 The Simultaneous Perturbation Stochastic Approximation Algorithm-SPSA*

The simultaneous perturbation and stochastic approximation (SPSA) algorithm was introduced by Spall [49, 50] as an improvement to Kiefer-Wolfowitz algorithm which approximates the gradient using standard finite-difference method [33, 49]. To approximate the gradient using the finite difference method, one needs to evaluate the cost function by running the simulator at the current point and at the perturbed points for each individual control variable, therefore, the number of simulation runs required is

equal to the problem dimension plus one. When the system is large, i.e., there are many control variables to adjust in the production optimization problem, the algorithms with the finite-difference gradient will be very inefficient. The SPSA algorithm mimics the finite-difference method for gradient calculation. However, instead of perturbing each control variable at a time, the SPSA algorithm simultaneously perturbs all the variables in a stochastic way, which requires only two simulation runs if one-sided perturbation is used or three simulation runs if two-sided perturbation is used. Due to the fact that the perturbation vector is stochastic, the search direction in the SPSA algorithm seems to be random. However, Spall [49, 50] shows that the SPSA gradient is always uphill in the vicinity of the current iterate when the perturbation is sufficiently small and the expectation of the SPSA gradient is the true gradient when the perturbation size approaches zero.

The SPSA algorithm was first introduced into the petroleum engineering literature by Gao et al. [25, 26] for history matching. In their implementation, the elements in the random perturbation vector are samples from a symmetric $\pm 1$ Bernoulli distribution, i.e., each element can take either 1 or -1 and the probability of taking 1 or -1 is 50%. As the reservoir porosity and permeability fields in the examples follow Gaussian distribution, the estimated reservoir models using this SPSA gradient does not give any geological realism. The estimated reservoir models was then improved when the SPSA gradient is smoothed with the prior covariance matrix of the reservoir property fields. This algorithm was denoted as the simple-second order SPSA [26]. Gao et al. [26] also tested the adaptive SPSA algorithm [51], which estimates an approximate Hessian matrix with simultaneous approximation as in the SPSA gradient calculation. The results are worse than that of the simple second-order SPSA algorithm. Li and Reynolds [36] further improved the SPSA algorithm using the unconditional realizations from the prior Gaussian probability density function (pdf) as the random perturbation vector. This algorithm is denoted as SGSD (stochastic Gaussian search direction) algorithm in Li and Reynolds [36]. For the production optimization problem, Bangerth et al.

[5] was the first one to use an integer SPSA for well placement optimization in oil reservoirs. Wang et al. [52] extended the SPSA algorithm developed in Gao et al. [26] to the optimal well control problem, in which the individual well controls are adjusted to maximize the net-present-value (NPV). Inspired by the fact that the expectation of the SPSA gradient is approximately the true gradient, Wang et al. [52] were able to obtain the same NPV using the an average of 5 SPSA gradients as the one obtained using the true gradient, although the former took much more simulation runs. Zhao et al. [56] also applied the SPSA algorithm to the production optimization problem, the SPSA algorithm gives better results than the particle swarm optimization (PSO), pattern search method guided by simplex gradient (SID-PSM), but inferior to their newly developed quadratic interpolation model with approximate gradient (QIM-AG).

Jia et al [32] used the basic SPSA algorithm in the SAGD process for history matching. Their history matching exercise in the SAGD process was done in a 2D homogeneous reservoir with single wellpair. They tried to match the production data by adjusting the permeability and porosity in the reservoir. Results seem to be in good agreement with the true model. This study will focus on the application of the newly developed SPSA algorithm with Gaussian perturbation to the SAGD production optimization.

### *1.1.4 Ensemble-Based Optimization- EnOpt*

The ensemble-based optimization (EnOpt) method for production optimization derives the approximate gradient using the cross-covariance between NPV and control vector. This covariance matrix is approximated in a standard statistical way with an ensemble of NPV values obtained by running the simulator using an ensemble of random control vectors around the current estimated optimal control. The idea is conceptually based on the result in Reynolds et al. [44] that the analysis step in the ensemble Kalman filter (EnKF) method is similar to performing to one Gauss-Newton iteration using an average gradient (or sensitivity matrix) derived from the ensemble.

The idea was first used for production optimization in Lorentzen et al. [37] and Nwaozo [41]. The EnOpt algorithm was then formalized by Chen et al. [18, 19] in the context of the closed-loop reservoir management. Chen and Oliver [17] applied the EnOpt method to the closed-loop reservoir management for the realistic Brugge case. In the EnOpt method, the key is to smooth the approximate gradient using a predefined covariance matrix. With smoothing, EnOpt is quite efficient and can generate realistic final optimal controls [56]. However, without any smoothing of the search direction, it generates final estimated controls which are suboptimal as shown in Wang et al. [52].

## 1.2 Research Scope

The focus of this study is to optimize the SAGD operations using NPV as the objective function. As there is no adjoint gradient option available in the thermal simulator (STARS from CMG) that can simulate the SAGD processes, only derivative-free optimization algorithms can be applied. In this study, the simultaneous perturbation and stochastic approximation (SPSA) and ensemble-based optimization (EnOpt) developed in the TUPREP research group will be tested. In this study, the well controls are steam injection rates and the production well bottomhole pressures. Two examples with a single wellpair case were considered in this study.

CHAPTER 2

# METHODOLOGY

## 2.1 Problem Formulation

In the production optimization problem, net-present-value (NPV) is usually used as the objective function to be maximized by adjusting well controls for the expected production life of the reservoir. For a given reservoir model, the NPV for the SAGD process is denoted as $J(u)$ and given by

$$J(u) = \sum_{n=1}^{N_t} \left[ \sum_{j=1}^{N_{\mathrm{PROD}}} (r_o q_{o,j}^n - r_w q_{w,j}^n) - \sum_{i=1}^{N_{\mathrm{INJ}}} r_{cwei} q_{cwei,i}^n \right] \frac{\Delta t^n}{(1+b)^{t^n/365}}, \tag{2.1}$$

where $u$ is the control vector which includes the steam injection rate and the producer bottomhole pressure for each control step; $N_t$ is the total number of simulation time steps; $q_{o,j}^n$ and $q_{w,j}^n$, respectively, denote the average oil and water production rates (STB/D) at the $j$th production well over the $n$th time step; $\Delta t^n$ is the $n$th simulation time step (day) and $t^n$ is the cumulative time (day) up to the $n$th simulation time step; $q_{cwei,i}^n$ is the average cold water equivalent steam injection rate at the $j$th injection well over the $n$th simulation time step; $N_{\mathrm{PROD}}$ is the total number of production wells and $N_{\mathrm{INJ}}$ is the total number of injection wells; $r_o$ and $r_w$ are the oil revenue and produced water treatment costs (\$/STB); $r_{cwei}$ is the cold water equivalent (CWE) steam injection cost (\$/STB) including the steam generation and transportation; $b$ is the annual discount rate.

Only bound constraints are considered in this study, so the maximization problem is defined as

$$\max_u J(u), \tag{2.2}$$

subject to bound constraints

$$u^{\text{low}} \leq u \leq u^{\text{up}}, \tag{2.3}$$

where $u^{\text{low}}$ and $u^{\text{up}}$ represent the lower and upper bounds for well controls.

In this work, the log-transformation is applied during optimization to enforce upper and lower bound constraints [27]. For the $i^{th}$ control variable $u_i$, the transformed variable $s_i$ is

$$s_i = \ln\left(\frac{u_i - u_i^{\text{low}}}{u_i^{\text{up}} - u_i}\right). \tag{2.4}$$

With the log-transformation, the constrained optimization problem is converted to an unconstrained optimization problem; when $u_i$ approaches its lower bound $u^{\text{low}}$, $s_i$ approaches $-\infty$ and when $u_i$ approaches its upper bound $u^{\text{up}}$, $s_i$ approaches $+\infty$. The optimization is done in the transformed domain and the updated variables are transformed back to the original domain at each iteration before they are given to the reservoir simulator. The inverse log-transformation is,

$$u_i = \frac{\exp(s_i)u_i^{\text{up}} + u_i^{\text{low}}}{1 + \exp(s_i)} \quad \text{for} \quad s_i < 0, \tag{2.5}$$

and

$$u_i = \frac{u_i^{\text{up}} + \exp(-s_i)u_i^{\text{low}}}{1 + \exp(-s_i)} \quad \text{for} \quad s_i > 0. \tag{2.6}$$

Simple truncation may also be used to keep all the control variables within the bounds, i.e., at each iteration, when a control variable is out of bound with the current stepsize, that variable is set to the bound value. This truncation is actually the gradient projection method on the active bound constraints[40]. The tests in Zhao et al.[56] show that log-transformation yields faster convergence than the simple truncation, so this study applies the log-transformation.

The following two sections give an account of the two algorithms (SPSA and EnOpt) used in this study.

## 2.2 SPSA Algorithm

The SPSA algorithm is used to iteratively maximize the NPV, $J(s(u))$ with the following equation

$$s^{l+1} = s^l + a_l \widehat{g}(s^l), \tag{2.7}$$

where $a_l$ is the stepsize. Note that the optimization is done in the log-domain on transformed vector $s$. The SPSA gradient with respect to the transformed control vector $s$ at the $l$th iteration, $\widehat{g}(s)$ can be calculated using one-sided perturbation

$$\widehat{g}(s^l) = \frac{J(s^l + c^l\Delta) - J(s^l)}{c^l}\Delta^{-1}, \tag{2.8}$$

or two-sided perturbation

$$\widehat{g}(s^l) = \frac{J(s^l + c^l\Delta) - J(s^l - c^l\Delta)}{2c^l}\Delta^{-1}. \tag{2.9}$$

Note that the "inverse" of vector $\Delta$ is an element-wise inverse, i.e., $\Delta^{-1} = [\frac{1}{\Delta_1}, \frac{1}{\Delta_2}, \cdots, \frac{1}{\Delta_{N_c}}]$. Here, $N_c$ is the number of controls or the dimension of the transformed control vector $s$. The above SPSA gradient calculation mimics that of the finite-difference method. The SPSA gradient requires one additional simulation run for the one-sided perturbation (Eq. 2.8) to evaluate $J(s^l + c^l\Delta)$ except the NPV at the current estimated optimal point $J(s^l)$ or two additional simulation runs for the two-sided perturbation (Eq. 2.9) to evaluate $J(s^l + c^l\Delta)$ and $J(s^l - c^l\Delta)$. However, the gradient calculation using the one-sided finite-difference method requires $N_c + 1$ number of simulation runs, i.e., each component of the gradient vector requires one additional simulation run

$$\frac{\partial J}{\partial s_i}(s^l) = \frac{J(s^l + ce_i) - J(s^l)}{c^l}, \tag{2.10}$$

where $e_i$ is a vector whose $i$th element is 1 and all other elements are zero.

As the SPSA gradient is obtained by simultaneously perturbing all the compo-

nents once, it does not calculate the true gradient as does the finite-difference method. However, the following shows that the expectation of the SPSA gradient is approximately the true gradient as long as the perturbation vector satisfies certain conditions. Taking the Taylor series expansion of $J(s^l + c^l\Delta)$ around $s^l$ yields

$$J(s^l + c^l\Delta) = J(s^l) + c^l\Delta^T g(s^l) + O((c^l)^2). \tag{2.11}$$

Substituting Eq. 2.11 into Eq. 2.8 yields

$$\widehat{g}(s^l) = \Delta^{-1}\Delta^T g(s^l) + O(c^l). \tag{2.12}$$

The expectation of the SPSA gradient is

$$E(\widehat{g}(s^l)) = E(\Delta^{-1}\Delta^T)g(s^l) + O(c^l), \tag{2.13}$$

where $\Delta^{-1}\Delta^T$ is

$$\Delta^{-1}\Delta^T = \begin{bmatrix} \Delta_1^{-1} \\ \Delta_2^{-1} \\ \vdots \\ \Delta_{N_c}^{-1} \end{bmatrix} [\Delta_1\ \Delta_2\ \cdots\ \Delta_{N_c}] = \begin{bmatrix} 1 & \frac{\Delta_2}{\Delta_1} & \cdots & \frac{\Delta_{N_c}}{\Delta_1} \\ \frac{\Delta_1}{\Delta_2} & 1 & \cdots & \frac{\Delta_{N_c}}{\Delta_2} \\ \vdots & \vdots & \ddots & \vdots \\ \frac{\Delta_1}{\Delta_{N_c}} & \frac{\Delta_2}{\Delta_{N_c}} & \cdots & 1 \end{bmatrix}. \tag{2.14}$$

As the components in vector $\Delta$ are independent random variables, there exists $E(\Delta_i) = 0$ and $E(\frac{1}{\Delta_j}) = 0$ as long as the random variable $\Delta_j$ is symmetric and does not take zero values. Therefore, for $i \neq j$

$$E(\frac{\Delta_i}{\Delta_j}) = E(\Delta_i)E(\frac{1}{\Delta_j}) = 0. \tag{2.15}$$

Taking the expectation of Eq. 2.14 gives an identity matrix, so Eq. 2.13 becomes

$$E(\widehat{g}(s^l)) = g(s^l) + O(c^l). \tag{2.16}$$

Eq. 2.16 shows that the expectation of the SPSA gradient is the true gradient with a bias of $O(c^l)$. The above derivation is done on the one-sided SPSA gradient. Similar proof can be applied to the two-sided SPSA gradient, in which case the bias is $O((c^l)^2)$.

When the SPSA algorithm was first introduced into the petroleum engineering literature, the elements of the random vector $\Delta$ are sampled from the symmetric $\pm 1$ Bernoulli distribution, i.e., $\Delta_i$ takes either 1 or -1 and the probability of taking one of them is 50%. In this case, $\Delta^{-1} = \Delta$, therefore, the SPSA gradient can be obtained directly using

$$\widehat{g}(s^l) = \frac{J(s^l + c^l\Delta) - J(s^l)}{c^l}\Delta, \tag{2.17}$$

or

$$\widehat{g}(s^l) = \frac{J(s^l + c^l\Delta) - J(s^l - c^l\Delta)}{2c^l}\Delta. \tag{2.18}$$

Motivated from Eqs. 2.17 and 2.18, Li and Reynolds [36] developed a stochastic Gaussian search direction (SGSD) method. In SGSD, the stochastic gradient is calculated using a perturbation vector sampled from the Gaussian distribution. The perturbation vector $\Delta$ in Eqs. 2.17 and 2.18 is substituted with Gaussian random vector $Z$ as

$$\widehat{g}(s^l) = \frac{J(s^l + c^l Z) - J(s^l)}{c^l} Z, \tag{2.19}$$

or

$$\widehat{g}(s^l) = \frac{J(s^l + c^l Z) - J(s^l - c^l Z)}{2c^l} Z. \tag{2.20}$$

It is shown in Li and Reynolds [36] that the expectation of the stochastic gradient in Eqs. 2.19 and 2.20 is the true gradient with a bias. In this study, all the examples were run with the one-sided perturbation as in Eq. 2.19, so the follow-

ing discussion pertains to the stochastic gradient using the one-sided perturbation. To obtain smooth controls over time, the perturbation vector $Z$ can be sampled from a Gaussian distribution which bears correlation in time for the controls of each well. For a production optimization problem with $N_w$ wells, perturbation vector $Z = [(Z^1)^T, (Z^2)^T, \cdots, (Z^k)^T, \cdots, (Z^{N_w})^T]^T$, where $Z^k$ represents the perturbation vector corresponding to the $k$th well. The perturbation vector for the $k$th well $Z^k$ is calculated by

$$Z^k = C_{s_k}^{\frac{1}{2}} \xi^k, \tag{2.21}$$

where $\xi^k$ is a vector of standard random normal deviates which has the same dimension as $s_k$; $C_{s_k}^{\frac{1}{2}}$ represents the square root of the covariance matrix $C_{s_k}$ for the controls of the $k$th well obtained using the Cholesky decomposition.

In this study, the covariance matrix $C_{s_k}$ is obtained using the spherical covariance function defined as

$$cov(s_{k,i}, s_{k,j}) = \begin{cases} 0\,, & \text{if} \quad |i-j| \geq \mathrm{T} \\ \sigma^2 \left[1 - \frac{3}{2}\frac{|i-j|}{T} + \frac{1}{2}\frac{|i-j|^3}{T^3}\right], & \text{if} \quad |i-j| < \mathrm{T} \end{cases}, \tag{2.22}$$

where $T$ is the number of control steps over which control variables are correlated in time and $\sigma$ is the standard deviation.

For a correlated perturbation vector, the expectation of the stochastic gradient in Eq. 2.19 is approximately equal to the covariance matrix ($C_s$) times the true gradient ($g(s)$), i.e.,

$$E(\widehat{g}(s^l)) \approx C_s g(s^l), \tag{2.23}$$

where $C_s$ is

$$C_s = \begin{bmatrix} C_{s_1} & & & \\ & C_{s_2} & & \\ & & \ddots & \\ & & & C_{s_{N_w}} \end{bmatrix}. \tag{2.24}$$

Due to this property, the search direction $\widehat{g}(s^l)$ in Eq. 2.7 is replaced with an average of several stochastic gradients $\overline{\widehat{g}}$.

$$\overline{\widehat{g}} = \frac{1}{N}\sum_{k=1}^{N}\widehat{g}_k(s), \tag{2.25}$$

where $N$ is the number of stochastic gradients. In this study, $N = 6$. Then Eq. 2.7 becomes

$$s^{l+1} = s^l + a_l\overline{\widehat{g}}(s^l). \tag{2.26}$$

The convergence proof for the original SPSA algorithm requires the perturbation size $c^l$ and the stepsize $a_l$ to go to zero as $l \to \infty$ [49] in a such way that

$$\sum_{l=0}^{\infty} a_l = \infty \quad \text{and} \quad \sum_{l=0}^{\infty}\left(\frac{a_l}{c^l}\right)^2 < \infty. \tag{2.27}$$

Spall [49, 50] suggested that $a_l$ and $c^l$ are calculated as

$$a_l = \frac{a}{(l+1+A)^{\alpha}}, \tag{2.28}$$

and

$$c^l = \frac{c_0}{(l+1)^{\gamma}}. \tag{2.29}$$

With this formulation, the convergence proof [49] also requires $\alpha - 2\gamma > 0$ and $3\gamma - 0.5\alpha \geq 0$. The values used in this study are $\alpha = 0.602$ and $\gamma = 0.101$, which are the same as the default values suggested by Spall [49, 50]. The values for parameters $c_0$, $a$ and $A$ are case dependent. The value for $c_0$ can be calculated based on the maximum number of iterations and the minimum value for the perturbation $c_{\min}$ as

$$c_0 = c_{\min}(N_{\text{MaxIt}} + 1)^{\gamma}. \tag{2.30}$$

Spall [49, 50] suggests that the value for $A$ is five to ten percent of the maximum

number of iterations. The average stochastic gradient $\overline{\widehat{g}}$ is multiplied by the covariance matrix $C_s$ to obtain additional smoothness for the updated control vector. To better determine the stepsize $a_l$, this study uses the normalized average stochastic gradient as the search direction, i.e.,

$$s^{l+1} = s^l + a_l \frac{C_s \overline{\widehat{g}}(s^l)}{\left\| C_s \overline{\widehat{g}}(s^l) \right\|_\infty}. \tag{2.31}$$

With the normalized search direction, the value for parameter $a$ is estimated by solving

$$a_0 = \frac{a}{(1+A)^\alpha}, \tag{2.32}$$

where $a_0$ is set as

$$a_0 = \beta \min_i \left\{ s_i^{\text{up}} - s_i^0, s_i^0 - s_i^{\text{low}} \right\}, \quad \text{where} \quad \beta \approx 0.5. \tag{2.33}$$

This study suggests that $s_i^{\text{up}}$ should take a value between 5 and 7, and $s_i^{\text{low}}$ should take a value between -7 and -5. The algorithm is terminated when the relative increase in the objective function is less than some specified threshold $\varepsilon$ value , i.e.,

$$\frac{|J(s^{l+1}) - J(s^l)|}{J(s^l)} \leq \varepsilon, \tag{2.34}$$

or when it reaches the defined maximum number of iterations.

## 2.3 EnOpt Algorithm

The basic EnOpt algorithm uses an estimated covariance matrix between NPV, $J(s)$ and transformed control vector $s$ as the search direction, i.e.,

$$s^{l+1} = s^l + \alpha_l C_{s,J}^{l+1}. \tag{2.35}$$

The covariance matrix $C_{s,J}^{l+1}$ is approximated by

$$C_{s,J}^{l+1} \approx \frac{1}{N-1}\sum_{j=1}^{N}(s_j^l - \overline{s^l})\left(J(s_j^l) - \overline{J(s^l)}\right)^T, \tag{2.36}$$

where $s_j^l$'s for $j = 1, \cdots, N$ are the perturbed transformed control vectors around $s^l$, i.e.,

$$s_j^l = s^l + C_s^{\frac{1}{2}}\xi,\ j = 1, \cdots, N. \tag{2.37}$$

Here $\xi$ is a vector of standard random normal deviates with dimension $N_c$. In Eq. 2.36, $\overline{s^l}$ represents the average of the perturbed control vectors, i.e.,

$$\overline{s^l} = \frac{1}{N}\sum_{j=1}^{N} s_j^l \approx s^l, \tag{2.38}$$

and $\overline{J(s^l)}$ represents the average of NPV evaluated at the perturbed control vectors, i.e.,

$$\overline{J(s^l)} = \frac{1}{N}\sum_{j=1}^{N} J(s_j^l). \tag{2.39}$$

Taking the Taylor series expansion of $J(s_j^l)$ around $\overline{s^l}$ yields

$$J(s_j^l) = J(\overline{s^l}) + g(\overline{s^l})^T(s_j^l - \overline{s^l}) + O(\|s_j^l - \overline{s^l}\|^2). \tag{2.40}$$

Substituting Eq. 2.40 into Eq. 2.36 yeilds

$$C_{s,J}^{l+1} \approx \frac{1}{N-1}\sum_{j=1}^{N}(s_j^l - \overline{s^l})\left(s_j^l - \overline{s^l}\right)^T g(\overline{s^l}). \tag{2.41}$$

Note that to arrive at Eq. 2.41, it is assumed that $J(\overline{s^l}) = \overline{J(s^l)}$ and the residual term in the Taylor series expansion of Eq. 2.40 is neglected.

Additional smoothness for the updated control vector can be obtained by mul-

tiplying the search direction by the covariance matrix $C_s$,

$$s^{l+1} = s^l + \alpha_l C_s C_{s,J}^{l+1} \approx s^l + \alpha_l C_s^2 g(s^l). \tag{2.42}$$

To better determine the stepsize, the search direction is normalized using its infinity norm, i.e.

$$s^{l+1} = s^l + \alpha_l \frac{C_s C_{s,J}^l}{\left\| C_s C_{s,J}^l \right\|_\infty}. \tag{2.43}$$

The initial stepsize is chosen as 1/10 of the smallest bound interval of the control vector [56], i.e.,

$$\alpha_l^0 = \beta \min_i \left\{ s_i^{\text{up}} - s_i^{\text{low}} \right\} \quad \text{where} \quad \beta = \frac{1}{10}. \tag{2.44}$$

The search direction in Eq. 2.43 of the EnOpt method is not necessarily an uphill direction. If $J(s^{l+1,k}) > J(s^l)$, then the control vector is updated and the process goes to the next iteration. If $J(s^{l+1,k}) \leq J(s^l)$, the stepsize is cut by half, i.e., $\alpha_l^{k+1} = \alpha_l^k/2$ and the control vector is updated using the new stepsize. If it does not improve the NPV after cutting stepsize 5 times, a new set of perturbed control vectors and hence a new search direction are generated around $s^l$. The algorithm is terminated in the same way as the SPSA algorithm, based on the number of iteration and the relative change of the objective function.

CHAPTER 3

# SAGD WITH SINGLE WELLPAIR

## 3.1 Model Description

The model in this chapter pertains to SAGD operations with a single wellpair, which involves one horizontal injector and one horizontal producer. This reservoir model is constructed based on the standard SAGD model provided by CMG and it is tested by CMOST optimization tool for production optimization. The reservoir has 50 simulation layers. The permeability is assumed to be homogeneous within each layer but is different from layer to layer. The layer permeability is shown in Fig. 3.1. The bottom 31 layers have a horizontal permeability of 4000 md and the horizontal permeability of the top layers decreases as depth decreases. The lowest permeability at the top 5 layers is 1000 md. The vertical permeability is different than the horizontal permeability, but it follows the same trend as the horizontal permeability. The detailed permeability values of the reservoir are given in Table 3.1. To save simulation run time during optimization, only a cross-section that is perpendicular to the horizontal wells is simulated, and the 2D simulation gridblock system is $101 \times 1 \times 50$. The size of each gridblock is 1 m$\times$10 m$\times$1 m. The top depth of the reservoir is 500 m, which is considered to be realistic for the tar sands in Canada [53].

The initial reservoir pressure at the reference depth (500 m), which is the top of the reservoir, is 2000 kPa and the initial temperature of the reservoir 10 °C throughout the reservoir. The producer is located at gridblock (51,1,49), which is close to the bottom of the reservoir and the injector is located at gridblock (51,1,45), which is 4 gridblocks (or 4 m) above the producer (Fig. 3.1).

Table 3.1: Layer permeabilities.

| Layers | $k_x = k_y$, mD | $k_z$, mD | $k_z/k_x$ |
|---|---|---|---|
| 1-10 | 1000 | 500 | 0.50 |
| 6-10 | 1500 | 700 | 0.47 |
| 11-15 | 1500 | 900 | 0.60 |
| 16-19 | 3000 | 1500 | 0.50 |
| 20-50 | 4000 | 2200 | 0.55 |

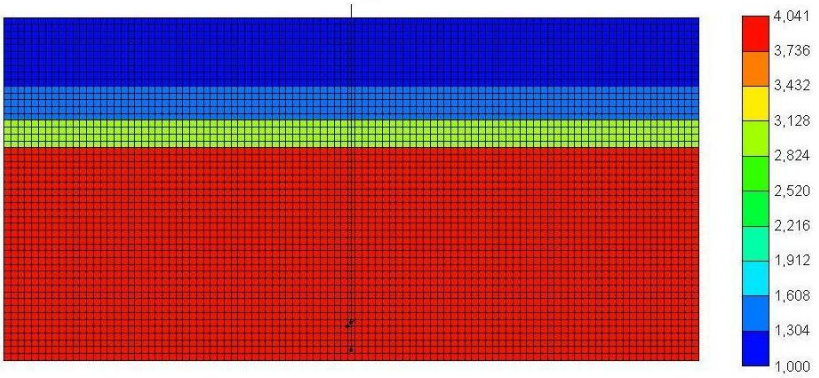


Figure 3.1: Horizontal permeability of the reservoir model.

One of the most important aspects in the SAGD operations is that the viscosity is a strong function of temperature. Fig. 3.2 shows this function used in this study. The viscosity has a wide range from $1.6 \times 10^6$ cp at the initial reservoir temperature down to about 20 cp at the injected steam temperature of 235 °C.

The SAGD process starts with a preheating period. During this period, the steam is injected into both wells through the tubing and then circulated back to surface through the annulus until communication is established between two horizontal wells. Assuming the steam quality and temperature do not change with time during this period, the formation around the wells should have the same temperature as the injected steam. In the simulator (CMG STARS), the preheating period can be modeled using "AUTOHEATER" option. With this option, one may set the well gridblock temperature to a constant using the keyword "TMPSET". In this case, a constant heat transfer rate is assigned using the "HEATR" option in STARS. The heater is turned

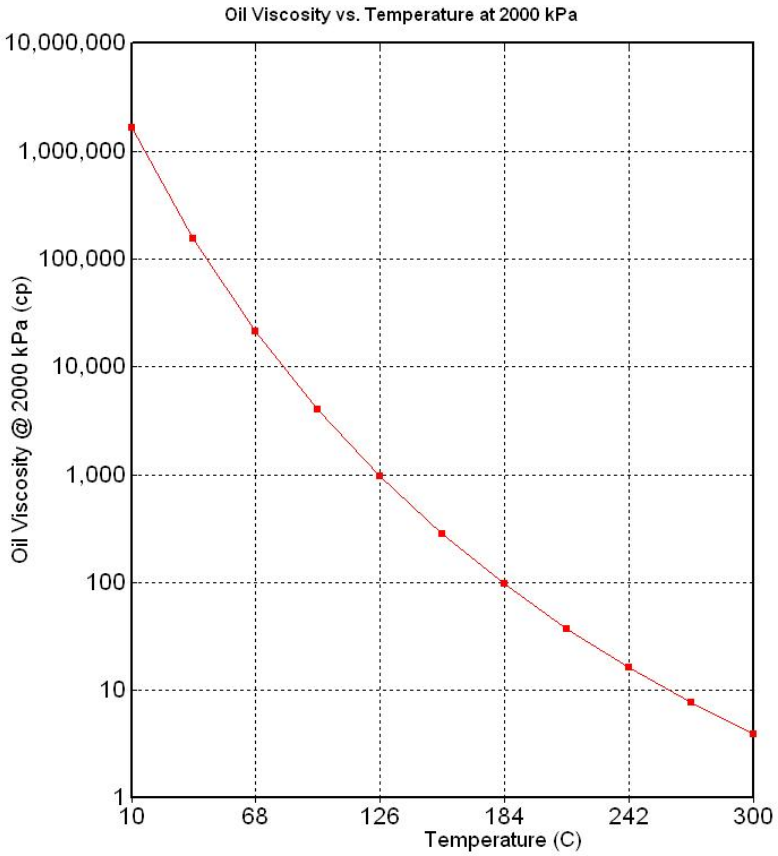


Figure 3.2: Oil viscosity as a function of temperature at 2000 kPa.

off automatically when the gridblock temperature exceeds the specified temperature. In this study, the "TMPSET" specified temperature is 225 °C for the well gridblocks. Note that once the well gridblock temperature drops below the "TMPSET" specified temperature, the heater is turned back on automatically. This can occur during late time when small steam injection rate is used. However, in this study, the "AUTO-HEATER" option is turned off after the preheating period of 400 days to avoid the frequent switches between heater on and off options. The model also considers the heat losses to the caprock and base formation using the "HLOSSPROP" option.

The injected steam temperature is 235 °C and the steam quality is 0.95 and both are kept constant through the entire reservoir production life. The total reservoir production life is 4383 days, which is divided into 22 control steps. The control stepsize

is 200 days for the first 21 control steps and the last control step is 183 days. With two wells, there are 44 control variables to be adjusted for production optimization. The oil revenue ($r_o$) per unit volume, produced water treatment cost ($r_w$) per unit volume, steam injection cost ($r_{cwei}$) per unit cold water equivalent (CWE) volume and annual discount rate ($b$) values used in Eq. 2.1 for NPV calculation are 50 \$/STB, 0.25 \$/STB, 10 \$/STB and 10%, respectively. The controls in this study are CWE steam injection rate for the injector and bottomhole pressure for the producer. The lower and upper bounds for the CWE steam injection rate are 0 $m^3$/day and 8 $m^3$/day, respectively and the maximum allowable bottomhole pressure for the injector is 10000 kPa. The production well bottomhole pressure has upper and lower bounds of 5000 kPa and 300 kPa.

## 3.2 Example 1

The controls for the first base case are constant 4 $m^3$/day CWE steam injection rate for injector and 1000 kPa bottomhole pressure for producer. The final oil saturation distribution at the end of the production life for the base case is shown in Fig. 3.3. The oil recovery factor for this base case is about 10.5% with a negative NPV of -\$4.36 $\times 10^5$. As the displacement efficiency is quite high within the steam chamber and the oil saturation outside of the steam chamber is close to the initial value, the oil saturation distribution in Fig. 3.3 can actually give an indication of the steam chamber development. In this base case, the steam chamber at the end of the reservoir life is not fully developed and it does not reach the caprock. The major reason for this under-developed steam chamber is that live steam production occurs shortly after the production starts due to high pressure differential between the injector and producer. This high pressure differential resulted in higher initial production rate hence no liquid pool, which forms the barrier that prevents steam production. Without the liquid pool, most injected steam will go directly to the producer and circulate back to the surface without even touching the cold tar sands. From heat management point view, this

is a waste of energy. The steam circulation through the producer is also indicated in the well gridblock temperature plot in Fig. 3.4. The temperature difference between the injector well gridblock (51,1, 45) and the producer well gridblock (51,1,45) is only about 3 to 4 °C after about day 500, which clearly indicates steam production. The cumulative steam oil ratio (cSOR) for the base case is about 17.4, which is another indicator of the inefficient energy usage in the base case.

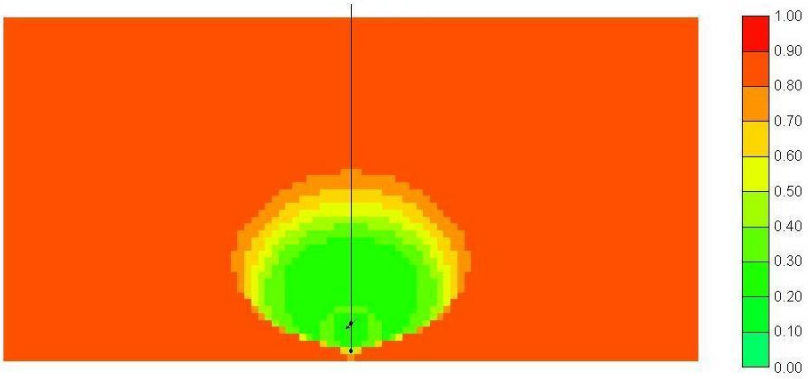


Figure 3.3: Remaining oil saturation distribution of the base case, Example 1.

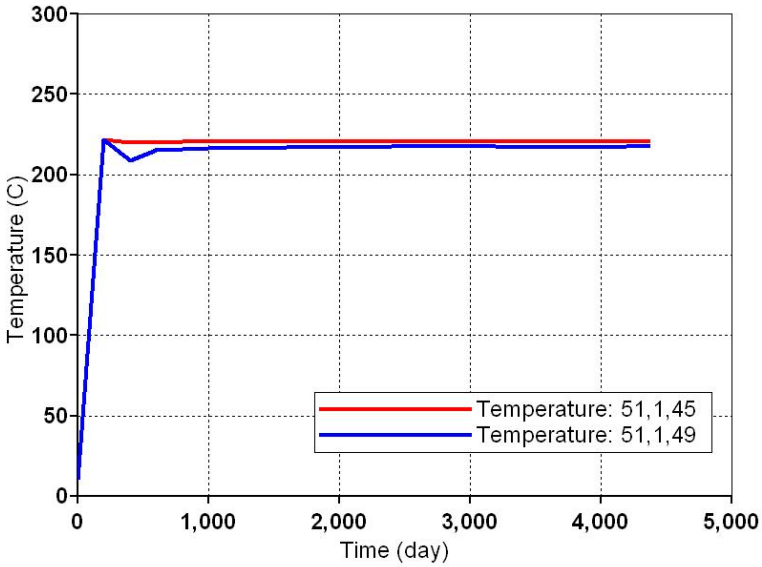


Figure 3.4: The temperature profile for the well gridblocks, base case of Example 1.

To improve heat management, usually the SAGD process applies the steam trap control using subcool, in which the temperature difference between the injected steam

and the produced fluids is kept above a certain value. This can also be viewed as a reactive control. Due to large pressure differential between the injector and producer in the base case, the producer produces at high rate at the beginning, which tends to drain the steam condensate and mobilized oil. With a small or no liquid pool between the injector and producer, some injected steam will flow directly to the producer and hence results in a decreasing subcool temperature. When this subcool is lower than the specified value, the production well bottomhole pressure is increased and the production rate is decreased to ensure that the subcool is kept at or above the specified value. As long as the specified value for subcool is large enough, no steam can be produced directly. In the simulator (STARS), the subcool control is enforced with keyword "STEAMTRAP" as a secondary constraint to the production well. In this study, the subcool reactive control is used as the reference case, which is compared with the final optimal controls obtained using SPSA and EnOpt.

Fig. 3.5 presents the NPV and cSOR obtained using different subcool temperatures as a secondary constraint. The NPV increases with increasing subcool up to 30 °C as more heat is retained in the reservoir to mobilize more oil. When the subcool further increases more liquid (steam condensate and mobilized oil) accumulates around the producer that reduces the productivity as oil cools down and slows down the steam chamber growth with less contact area (see Figs. 1.1 and 1.2). In order to avoid the problem of determining the optimum subcool value to be used through the production life of the reservoir, bottomhole pressure can be used as the production well operating control. Summary of the effect of the subcool value on the production performance is given in Table 3.2.

The subcool temperature for the reactive control in this study is chosen to be 20 °C based on the literature and typical values used in the field practice [23, 31]. The temperature profile of the well gridblocks of the injector and producer for the reactive control is shown in Fig. 3.6.

The SPSA and EnOpt algorithms are applied to optimize NPV in this study

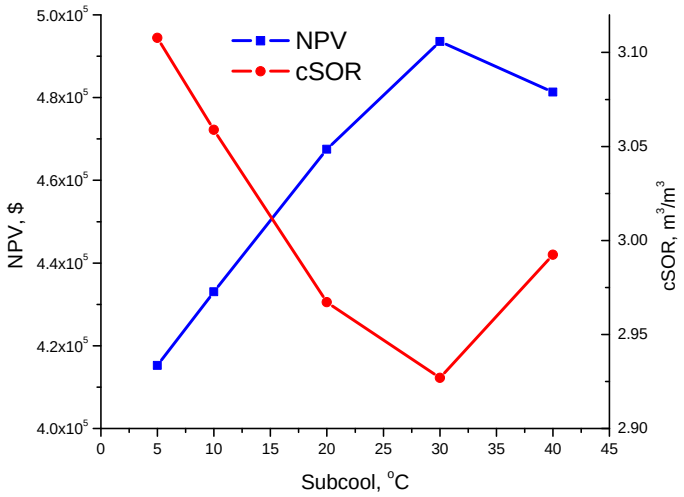


Figure 3.5: Effect of the subcool temperature on the production performance.

Table 3.2: Summary of the subcool value effect on the production.

| Subcool, °C | Cum. Oil Prod., $m^3$ | Cum. Steam Inj. (CWE), $m^3$ | cSOR |
|---|---|---|---|
| 5 | 35478 | 110263 | 3.12 |
| 10 | 36046 | 110263 | 3.06 |
| 20 | 37161 | 110263 | 2.97 |
| 30 | 37677 | 110263 | 2.93 |
| 40 | 36848 | 110263 | 2.99 |

using the base case as the initial guess of controls. For both optimization algorithms, log-transformation is applied to ensure the controls are within bounds and the controls of each well has a correlation time lag of 5, i.e., $T = 5$ in Eq. 2.22 with spherical correlation function. The SPSA algorithm uses an average of 6 SPSA gradients, i.e., $N = 6$ in Eq. 2.25. The ensemble size for the EnOpt algorithm is 10, i.e., $N = 10$ in Eq. 2.36. Therefore, the SPSA algorithm requires 7 simulation runs at each iteration: 6 for the stochastic gradient calculation and 1 simulation run for the objective function evaluation. The EnOpt algorithm requires 11 simulation runs if no stepsize cut is required: 10 simulation runs for the cross-covariance $C_{U,J}$ matrix approximation and 1 simulation run for the NPV evaluation. However, if the cross-covariance is not an uphill direction, stepsize cuts may be applied, which may in turn require as many as

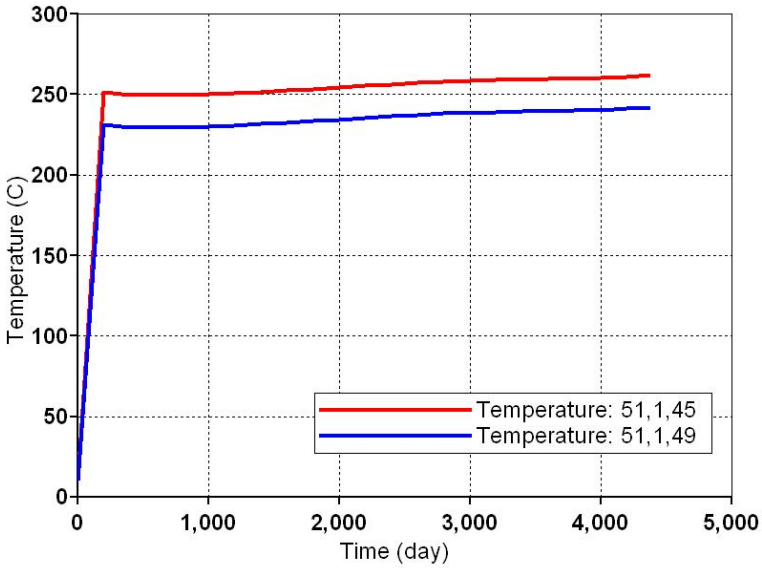


Figure 3.6: The temperature profile for the well gridblocks, reactive control of Example 1.

5 more simulation runs. The values for the parameters in the SPSA algorithm are $A = 5.0$ (Eq. 2.28), $a = 5.0$ (Eq. 2.28) and $c_0 = 0.1$ (Eq. 2.29). The initial stepsize for the EnOpt algorithm is $a^0 = 1.0$ (Eq. 2.44).

The final well controls obtained by the SPSA and EnOpt algorithms are shown in Figs. 3.7 and 3.8 compared with that of the subcool reactive control. The steam injection rates from the final optimal controls of the SPSA and EnOpt algorithms show similar behaviors: gradually increasing injection rate during early time and then a gradual decreasing steam injection rate after full development of the steam chamber. This complies with the results in the literature [6, 28, 29]. During the first 200 days, no steam is injected into the reservoir with the final controls of both SPSA and EnOpt. This time corresponds to the preheating period. Once there is mobilized oil around the wells and communication between the injector and producer is established, the steam injection rate is gradually increased in both cases till it reaches its highest point between day 1200 and 1400. At this point, the steam chamber has reached the caprock at the top of the reservoir and the SAGD process starts losing energy to the caprock through conduction. To reduce energy loss, the injection rate is gradually decreased

allowing the steam chamber to grow in the lateral direction.

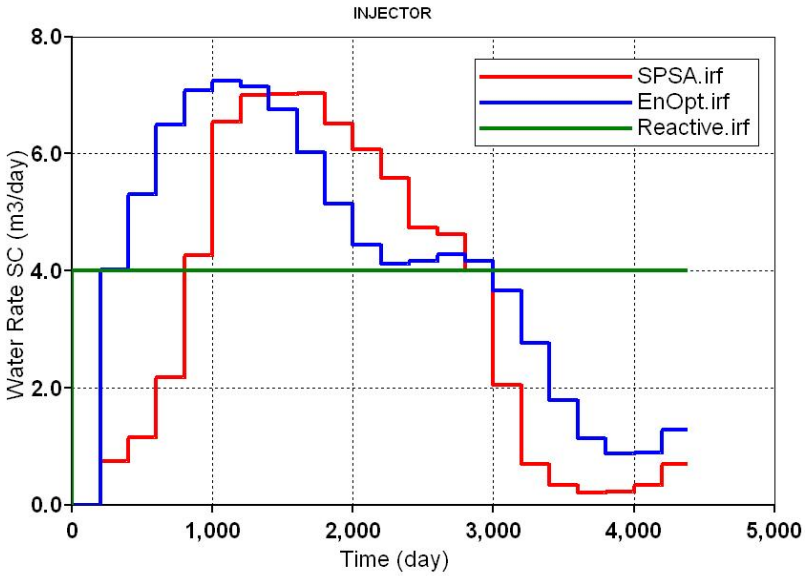


Figure 3.7: Final controls: CWE steam injection rate, Example 1.

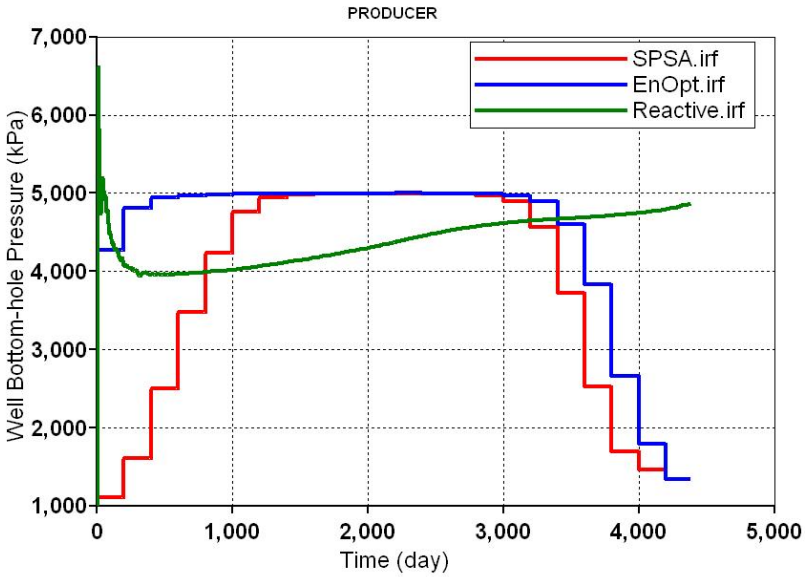


Figure 3.8: Final controls: producer bottomhole pressure, Example 1.

The production well bottomhole pressure control from SPSA and EnOpt (Fig. 3.8) show also similar behavior. The bottomhole pressure starts with a low value trying to produce as much oil as it can. Then it increases to its upper bound of 5000 psi and gradually decreases at the end of the process. Compared with SPSA, EnOpt bottom-

hole pressure has relatively high values at the beginning of the process and reaches its upper bound faster than SPSA. The bottomhole pressure control is somewhat synchronized with the corresponding steam injection rates: low steam injection rate to low production well bottomhole pressure and high steam injection rate to high production well bottomhole pressure. The change in the production well bottomhole pressure can prevent live steam production as in the subcool control. However, different than the subcool control, the steam injection rate is also adjusted to maximize the NPV with SPSA or EnOpt. In addition, there is no need to monitor the production fluid temperature and keep a constant subcool temperature during the production life of the reservoir. Figs. 3.9 and 3.10 show the temperature at the well gridblocks and the difference between these two gridblocks is the subcool. The figures show that the subcool temperature resulted from the optimized controls in both SPSA and Enopt varies between 13 °C and 60 °C. The reactive control forces constant cold water equivalent (CWE) steam injection rate of 4 $m^3$/day during the reservoir production life (Fig. 3.7). To minimize steam production, production well bottomhole pressure is adjusted to maintain a liquid pool around the producer. However, due to high steam injection rate during the early time of the production life, the oil production rate at early time is also higher than the optimized case from both SPSA and EnOpt, which can be seen from the cumulative oil production plots in Fig. 3.11. Therefore, the reactive control produces oil faster than the optimized cases. However, it might not be possible to inject at high steam rate before communication is established between the injector and producer without fracturing the reservoir, which will form a direct path for the steam to go directly to the producer and be detrimental to the SAGD process.

Fig. 3.12 shows the remaining oil saturation distribution at the end of the reservoir production life obtained by running the simulator with the final optimal controls from SPSA and EnOpt compared with the reactive control. The green area is the steam chamber while the red region is not yet touched by the injected steam. The subcool reactive control and the final optimal control obtained by the SPSA algorithm have

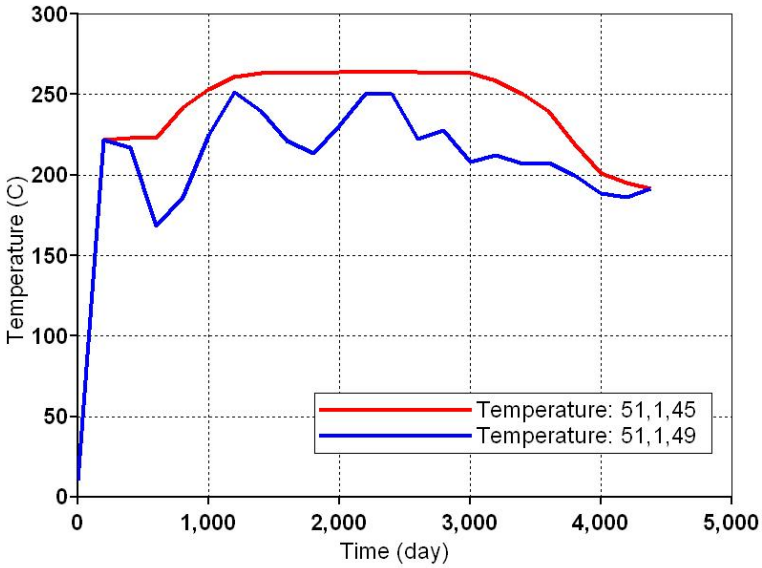


Figure 3.9: Well gridblock temperature, SPSA of Example 1.

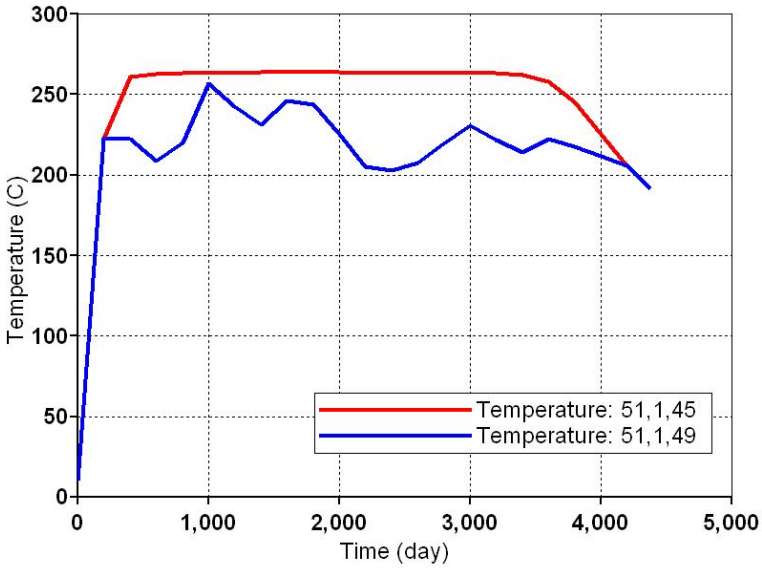


Figure 3.10: Well gridblock temperature, EnOpt of Example 1.

a steam chamber of similar size and oil recovery (about 64%), but the final optimal controls obtained by EnOpt gives the largest steam chamber growth, hence the high oil recovery of 74.21%.

The NPV as a function of iteration for SPSA (pink curve) and EnOpt (blue curve) is shown in Fig. 3.13 together with the NPV of the reactive control (green line). Note that the initial control from the base case gives a negative NPV due to limited

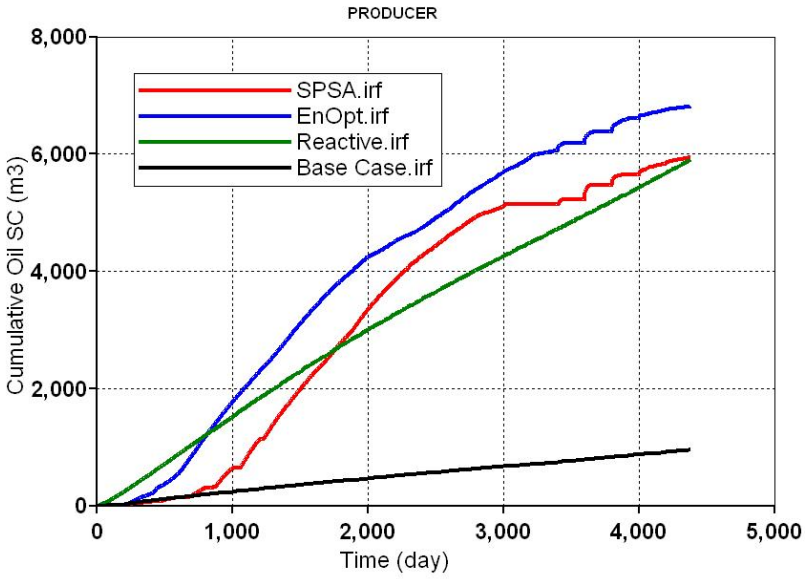


Figure 3.11: Cumulative oil production, Example 1.

steam chamber growth (Fig. 3.3). Starting with this negative NPV, SPSA improved the NPV to $\$5.60 \times 10^5$ and EnOPt improved the NPV to $\$6.30 \times 10^5$. While the reference case with the reactive control only gives about $\$4.68 \times 10^5$. Even though EnOpt required only 23 iterations and 288 simulation runs, it resulted in better NPV than SPSA, which required 51 iterations and 363 simulation runs. The summary of the performance of the algorithms is given in Table 3.3.

Table 3.3: Performance summary of the different algorithms, Example 1.

| Algorithm | Iterations | Simulation Runs | NPV, $ |
|---|---|---|---|
| SPSA | 51 | 363 | $5.60\times10^5$ |
| EnOpt | 23 | 283 | $6.30\times10^5$ |
| Reactive | - | - | $4.68\times10^5$ |

The oil production rate along with the production well bottomhole pressures obtained with the final optimal controls from SPSA and EnOpt are given in Figs. 3.14 and 3.15. In both cases, the oil rate gradually increases at early time and then it gradually declines once the production bottomhole pressure reaches it plateau. At the beginning of control steps 3-5 in Fig. 3.14, there is a short shut-in period shown as

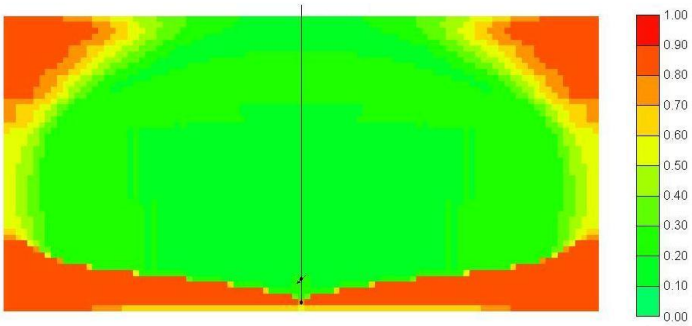


(a) Reactive case (RF:64.35%).

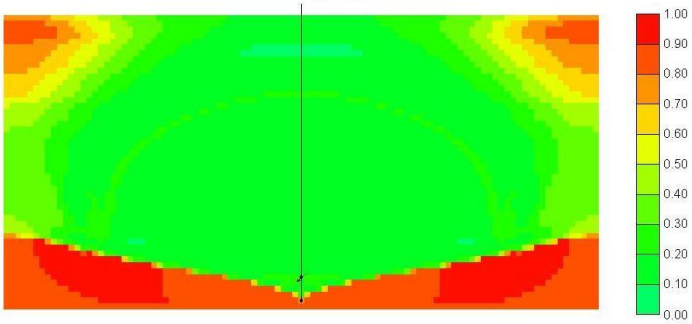


(b) SPSA (RF:64.79%).

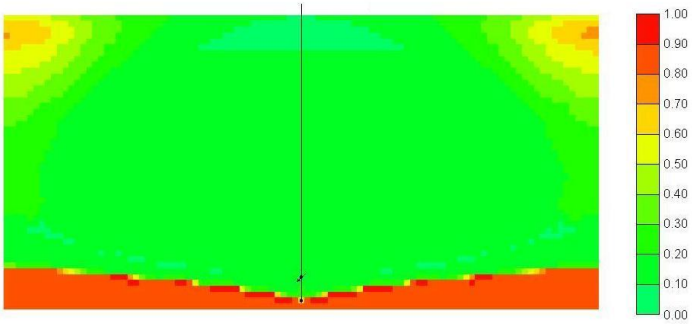


(c) EnOpt (RF:74.21%).

Figure 3.12: The remaining oil saturation distribution, Example 1.

zero oil rate as a result of the sudden increase in the bottomhole pressure from the control. While the final controls of EnOpt resulted in much smoother oil production rate during early time. At the end of the production life, the oil rate of both SPSA and EnOpt show some spiking high values at the beginning of each control step as a result of the abrupt bottomhole pressure drops. More control steps are needed to avoid such unrealistic abrupt changes.

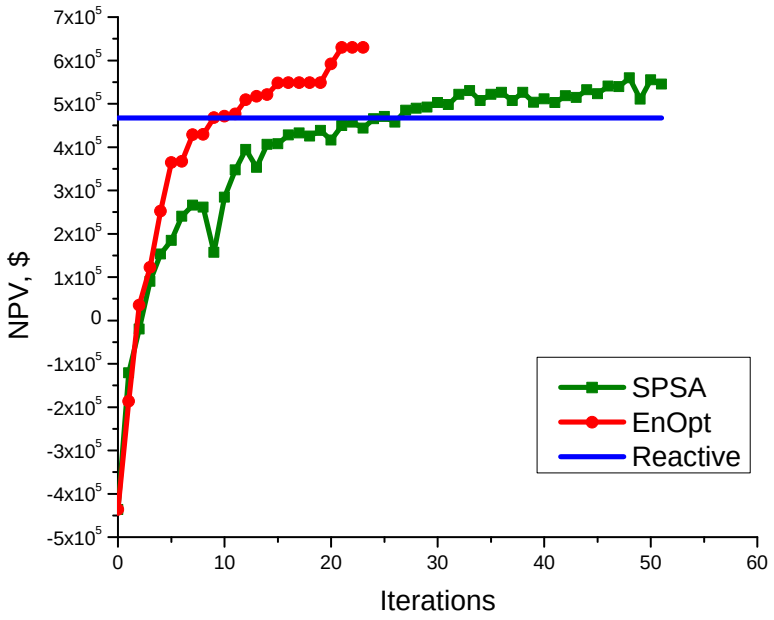


Figure 3.13: Resulting NPV for the SPSA, EnOpt and the reactive cases, Example 1.

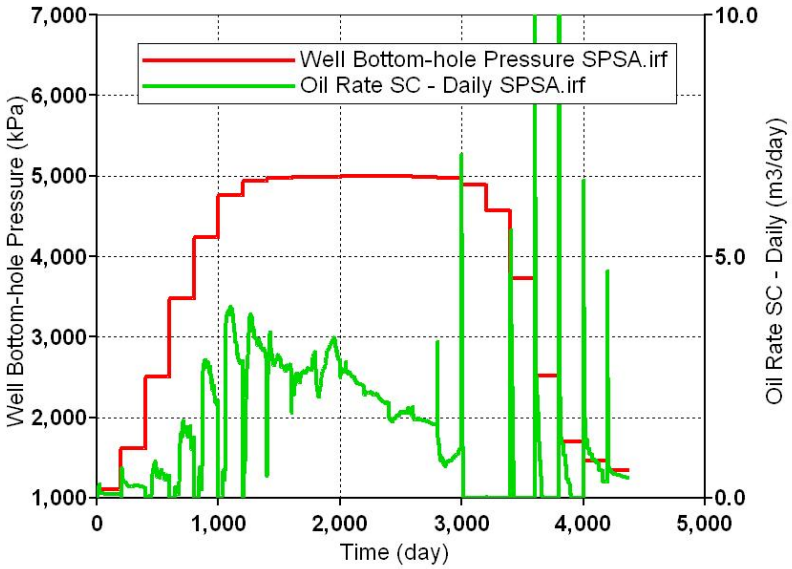


Figure 3.14: Oil rate and bottomhole pressure, SPSA of Example 1.

Fig. 3.16 presents the cumulative steam-oil ratio (cSOR) obtained by the final controls of SPSA, EnOPt and the reactive control. The cSOR trend is opposite during early time between the optimized cases from SPSA and EnOpt and the subcool reactive

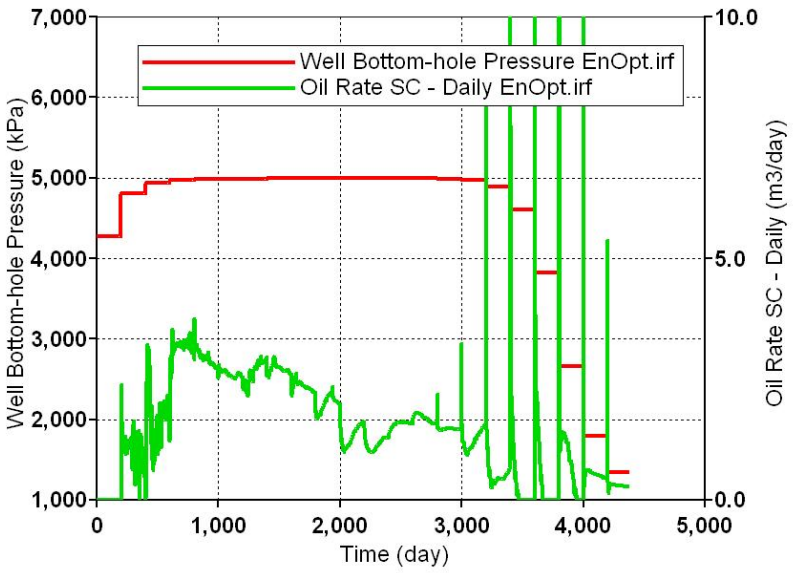


Figure 3.15: Oil rate and bottomhole pressure, EnOpt of Example 1.

control. The reactive control starts with a very high value of cSOR and gradually decreases while the cSOR from the optimal controls in SPSA and EnOpt is zero during the first 200 day of preheating period and increases gradually to a high value of about 3 to 4. The cSOR behavior after day 1000 is about the same for all three cases, but the reactive control gives the highest final cSOR. Summary of the cSOR values can be found in Table 3.4. Recall that the oil recovery with the reactive control is about the same as that of the optimized case obtained with SPSA, but the final NPV obtained with the optimal control from SPSA is about 20% higher than that of the reactive control as shown in Fig. 3.13 and Table 3.3. This is mainly because the final optimal control from SPSA injects less steam compared with the reactive control as shown in Table 3.4.

Table 3.4: cSOR summary, Example 1.

| Algorithm | Cum. Oil Prod., $m^3$ | Cum. Steam Inj. (CWE), $m^3$ | cSOR |
|---|---|---|---|
| SPSA | 37414 | 90548 | 2.42 |
| EnOpt | 42853 | 111596 | 2.60 |
| Reactive | 37160 | 110263 | 2.97 |
| Base case | 6058 | 105241 | 17.37 |

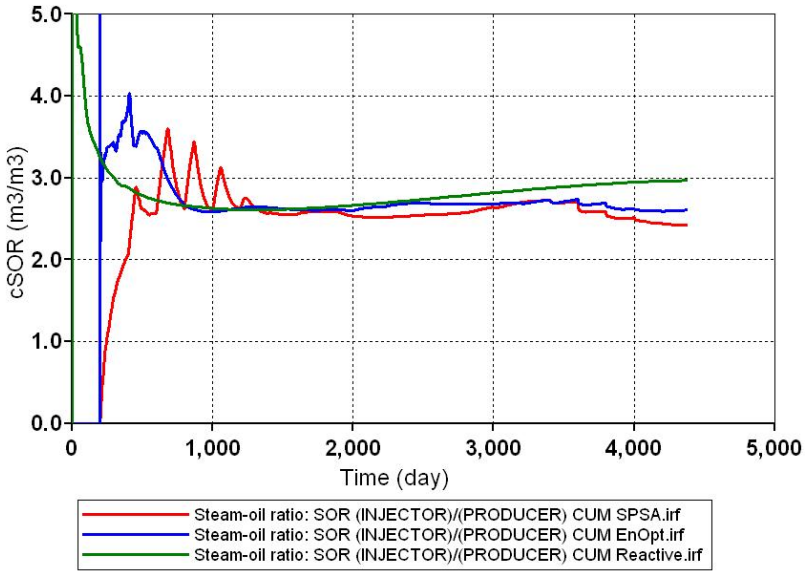


Figure 3.16: cSOR for SPSA, EnOpt and the reactive control, Example 1.

## 3.3 Example 2

In Example 1, the production optimization using SPSA and EnOpt started with a base case that has a constant CWE steam injection rate of 4 $m^3$/day and production well bottomhole pressure of 1000 psi, which resulted in a negative NPV. The reactive control with a subcool temperature of 20 °C gives a much higher NPV than the base case. As the simulation run for the SAGD process is very computationally expensive, Example 2 starts production optimization with a set of better initial well controls for SPSA and EnOpt. The initial well control for the CWE steam injection rate is 4 $m^3$/day and it is the same as the reactive control except for the first control step, which has a zero steam injection rate to mimic the preheating period with "AUTOHEATER" option on. The initial well controls on the production well bottomhole pressure are discretized from the reactive control as shown in Fig. 3.17. Using these controls as the base case, the subcool temperature is not constant any more, but varies with time as shown in Fig. 3.18. The comparison of the oil production rate and the cumulative oil production between this base case and the reactive control with subcool of 20 °C is shown in Figs. 3.19 and 3.20. Due to the discretization on the production well control

and zero injection rate during the first control step, the NPV dropped from $\$4.68 \times 10^5$ for reactive control to $\$4.18 \times 10^5$ for base case. It is also noticeable that there are some short shut-in period at the beginning of some control steps due to sudden increase of production well bottomhole pressure in the base case (Fig. 3.19), whereas reactive control gives a very smooth oil production rate.

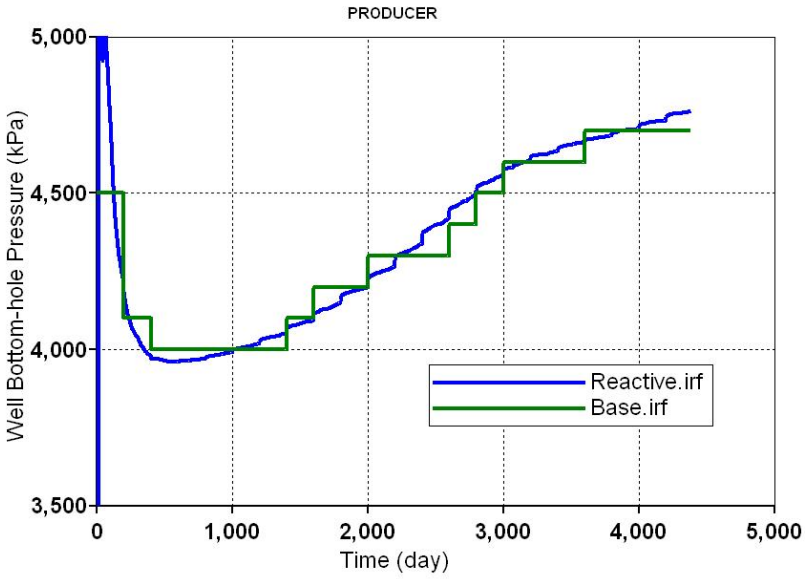


Figure 3.17: Bottomhole pressure of the base and reactive cases, Example 2.

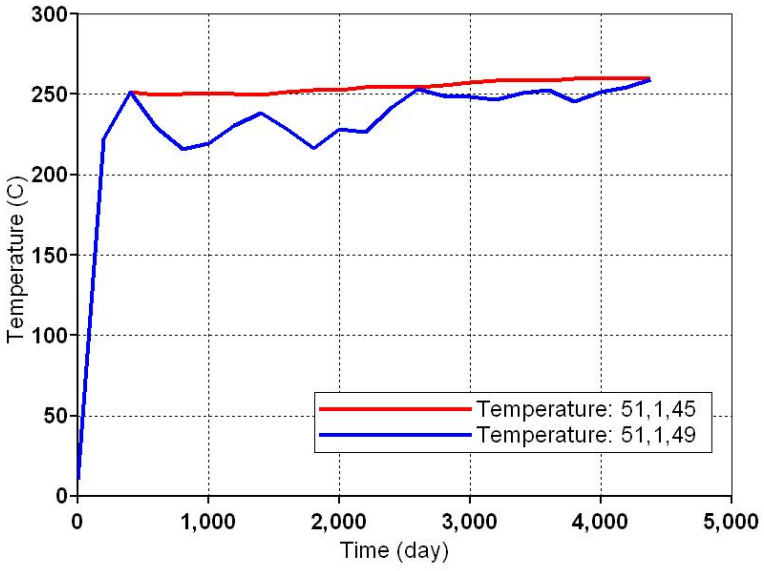


Figure 3.18: The base case subcool behavior, Example 2.

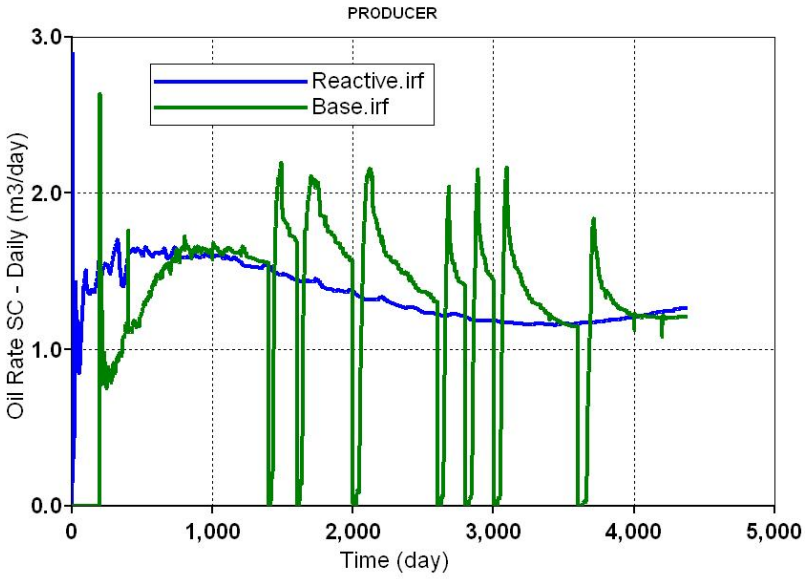


Figure 3.19: Oil production rates of the base and reactive cases, Example 2.

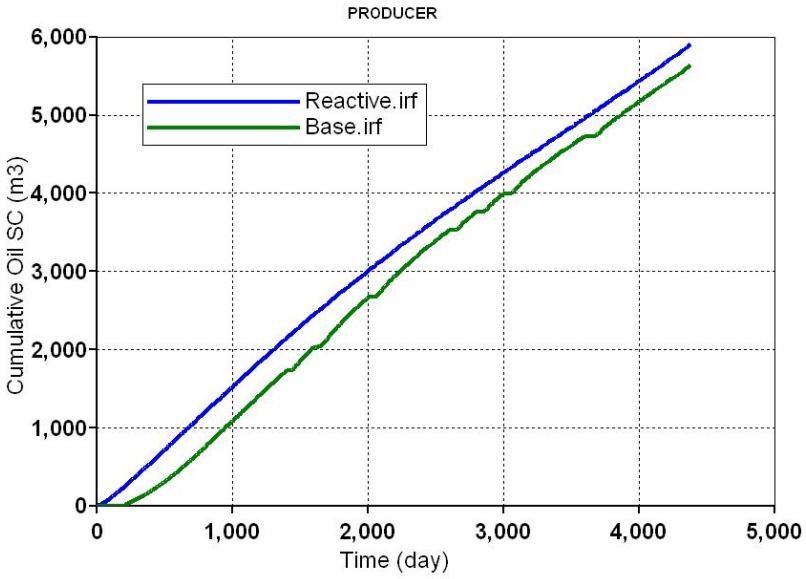


Figure 3.20: Cumulative oil production of the base and reactive cases, Example 2.

Both the SPSA and EnOpt algorithms are used for the production optimization. All the parameters used in this example are the same as those of Example 1, except that in SPSA $a = 2.0$ (Eq. 2.28), which is changed in order to achieve smaller stepsize as the given initial well controls are much closer to the bounds in this example.

The remaining oil saturation distribution obtained with the final optimal controls from SPSA and EnOpt is given in Fig. 3.21 compared to that of the base case.

SPSA and EnOpt improved the base case oil recovery factor from 61.37% to 77.02% and 76.43%, respectively. The final oil saturation distribution shows that the steam chamber is fully developed in both the vertical and lateral directions with the final optimal controls. The final optimal controls result in much higher final oil recovery in this case compared to Example 1 (Fig. 3.12).

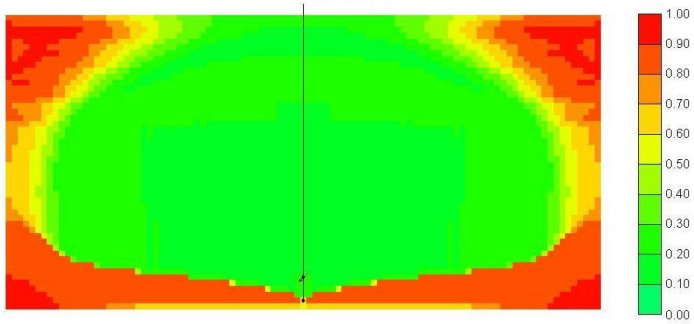


(a) Base case (RF:61.37%).

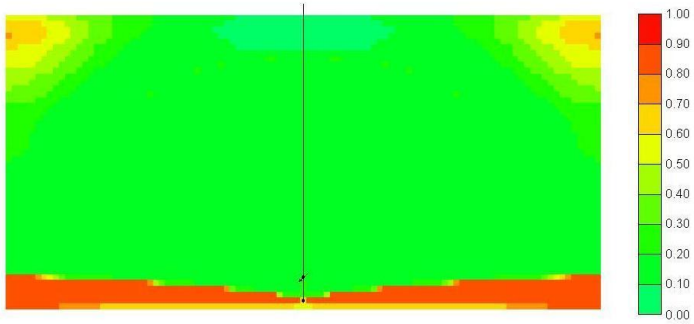


(b) SPSA (RF:77.02%).

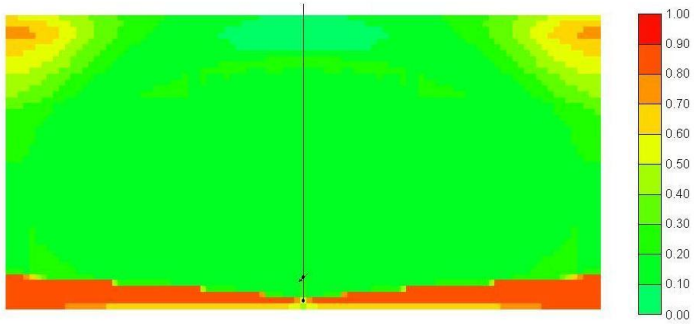


(c) EnOpt (RF:76.43%).

Figure 3.21: Remaining oil saturation distribution and RF for the SPSA, EnOpt and the base case, Example 2.

The well controls obtained by optimization and those of the base case are given

in Figs. 3.22 and 3.23. Both SPSA and EnOpt obtain a similar steam injection strategy as that of Example 1: preheating period with zero steam injection rate, then gradual increasing steam injection rate and then gradual declining steam injection rate. The production well bottomhole pressure controls of SPSA and EnOpt are similar, but they are very different than those of the base case. As the steam injection rate during early time was increased from the base case value of 4 $m^3$/day to a much higher level by optimization, the corresponding production well bottomhole pressure is also increased to prevent live steam production.

The oil production rate for both SPSA and EnOpt together with the base case are given in Fig. 3.24. Note that the oil production rate from the SPSA and EnOpt final optimal controls follow each other except for the spikes at the beginning of each control step. These spikes are due to sudden increase or decrease of the production well bottomhole pressure. The cumulative oil production is given in Fig. 3.25. The final optimal controls from SPSA and EnOpt give very close values of cumulative oil production which are much higher than that of the base case.

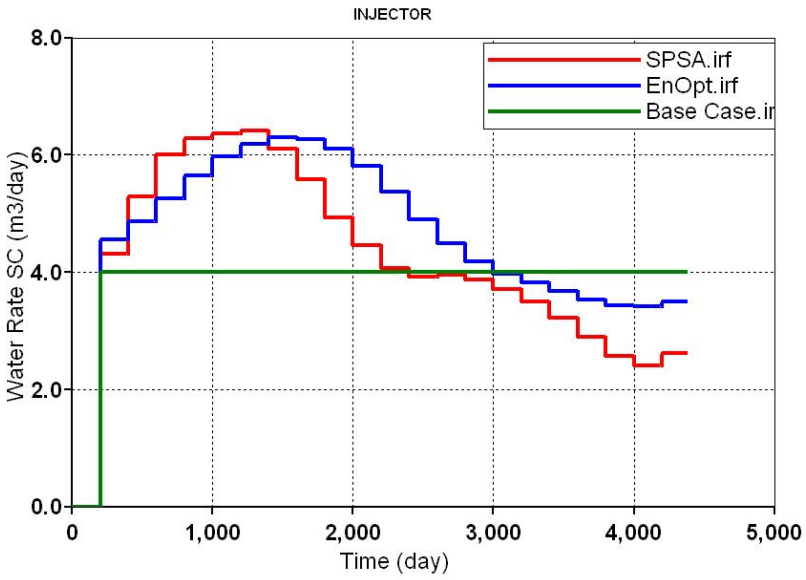


Figure 3.22: Final controls: CWE steam injection rates, Example 2.

Fig. 3.26 shows the NPV as a function of iterations for SPSA (blue curve) and

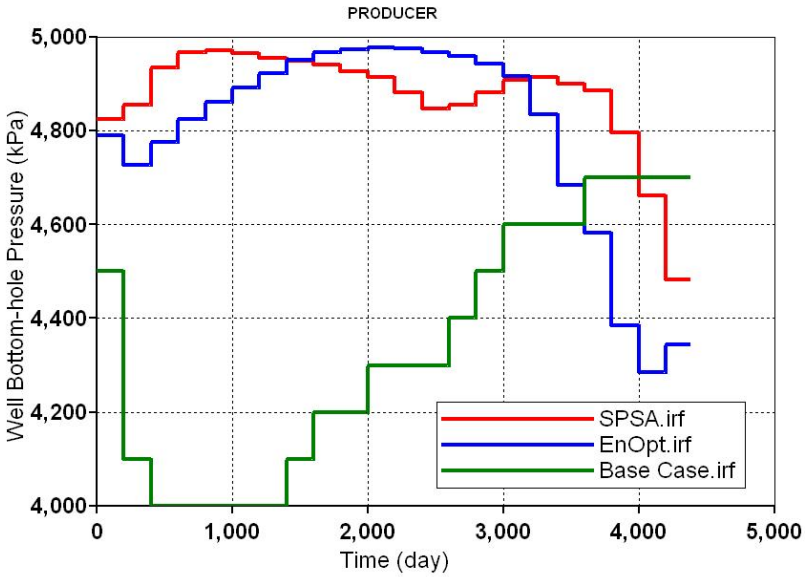


Figure 3.23: Final controls: producer bottomhole pressure, Example 2.

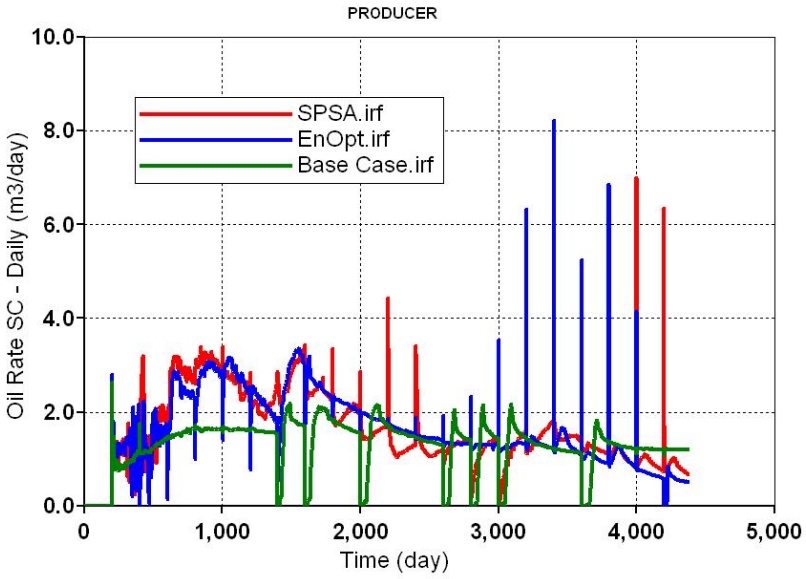


Figure 3.24: Oil production rates, Example 2.

EnOpt (pink curve). Note that the black straight line at the bottom is the NPV of the base case, which is the initial guess for the production optimization of both SPSA and EnOpt. Both SPSA and EnOpt improved NPV in the first 10 iterations. EnOpt failed to further improve NPV after it reaches a value of $\$5.88 \times 10^5$ in 14 iterations with 190 simulation runs while SPSA continued to improve the NPV to a value of $\$6.48 \times 10^5$ after 89 iterations (624 simulation runs). The summary of the performance

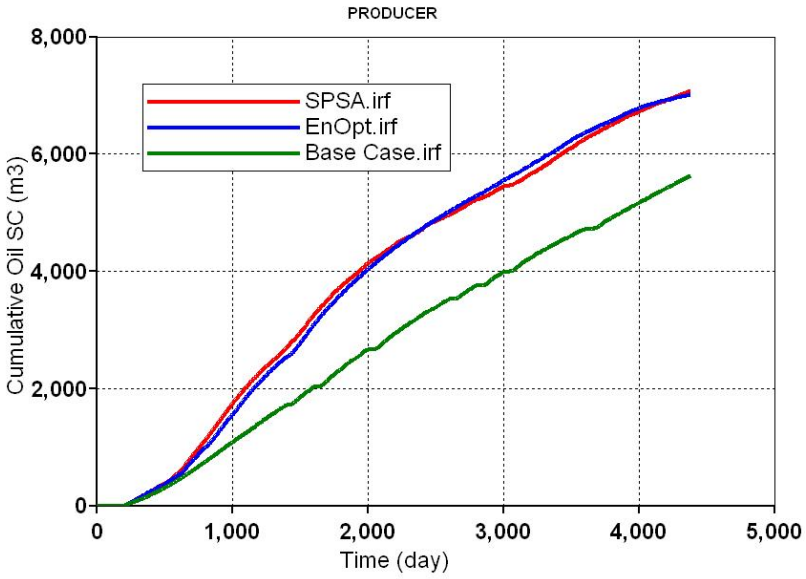


Figure 3.25: Cumulative oil production, Example 2.

of the algorithms is given in the Table 3.5. Recall that the cumulative oil production obtain by the final controls of SPSA and EnOpt is about the same (see Fig. 3.20). The significant difference in NPV is due to difference in the steam injection rates. Table 3.6 shows the cumulative steam injection in SPSA is significantly smaller than that in EnOpt. Similar behavior is also observed in cSOR. Fig. 3.27 presents the cSOR values for SPSA, EnOpt and the base case. All controls share similar behavior in cSOR, i.e., cSOR starts with a high value and gradually decreases.

Table 3.5: Performance summary of the different algorithms, Example 2.

| Algorithm | Iterations | Simulation Runs | NPV, $ |
|---|---|---|---|
| SPSA | 89 | 624 | $6.48\times10^5$ |
| EnOpt | 14 | 190 | $5.88\times10^5$ |
| Reactive | - | - | $4.18\times10^5$ |

The well gridblock temperature from the final controls in SPSA and EnOpt is given in Figs. 3.28 and 3.29. The subcool in the final controls of SPSA (Fig. 3.28) maintains a relatively constant value of about 60 °C over the production life while the subcool in EnOpt varies significantly with time. From day 2000 to 2500 and after day

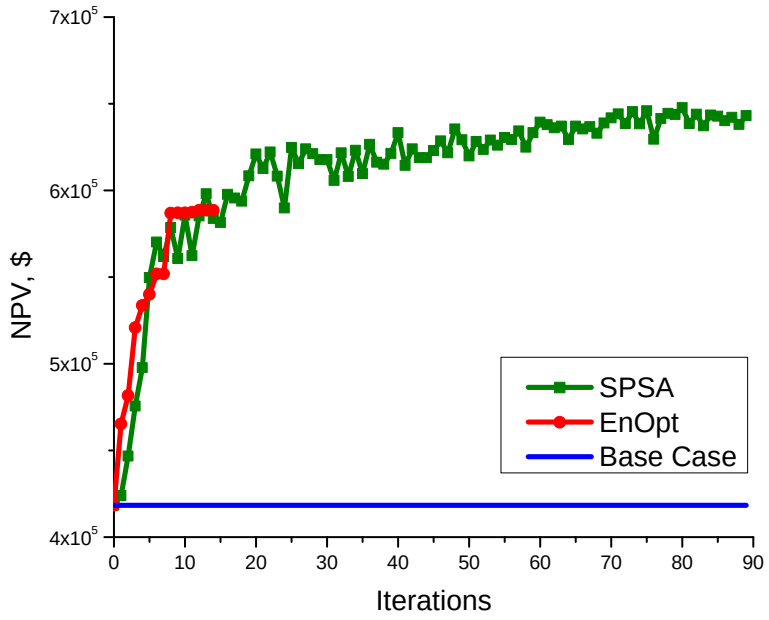


Figure 3.26: NPV of SPSA, EnOpt and the base case, Example 2.

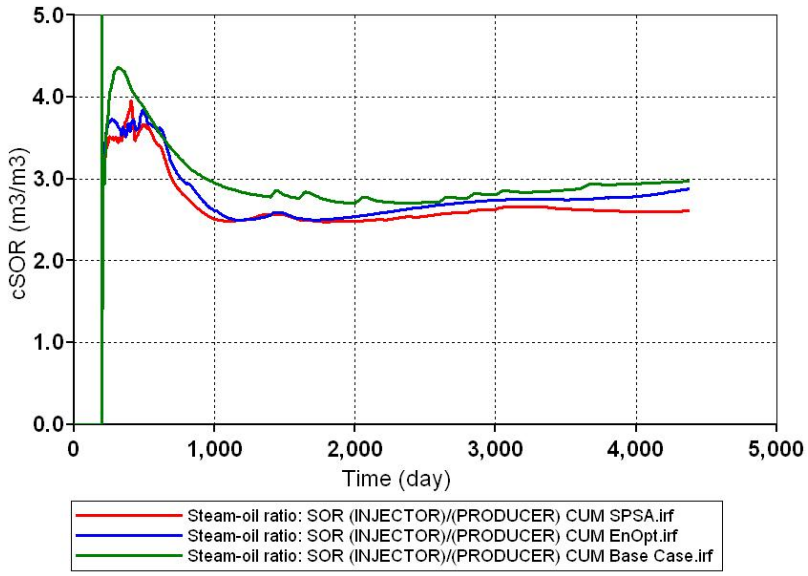


Figure 3.27: cSOR of SPSA, EnOpt and the base case, Example 2.

3300, the subcool in EnOpt is zero, which indicate that there is live steam production within these time periods. This is consistent with the cSOR behavior: SPSA has the smallest cSOR while the cSOR in EnOpt is much higher.

Table 3.6: cSOR summary, Example 2.

| Algorithm | Cum. Oil Prod., $m^3$ | Cum. Steam Inj. (CWE), $m^3$ | cSOR |
|---|---|---|---|
| SPSA | 44478 | 116052 | 2.61 |
| EnOpt | 44134 | 127027 | 2.88 |
| Base Case | 35439 | 105241 | 2.97 |

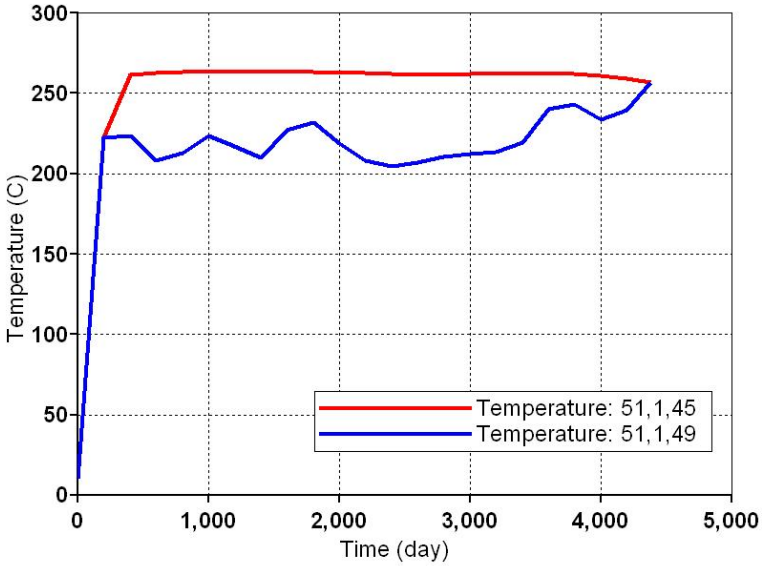


Figure 3.28: Well gridblock temperature, SPSA of Example 2.

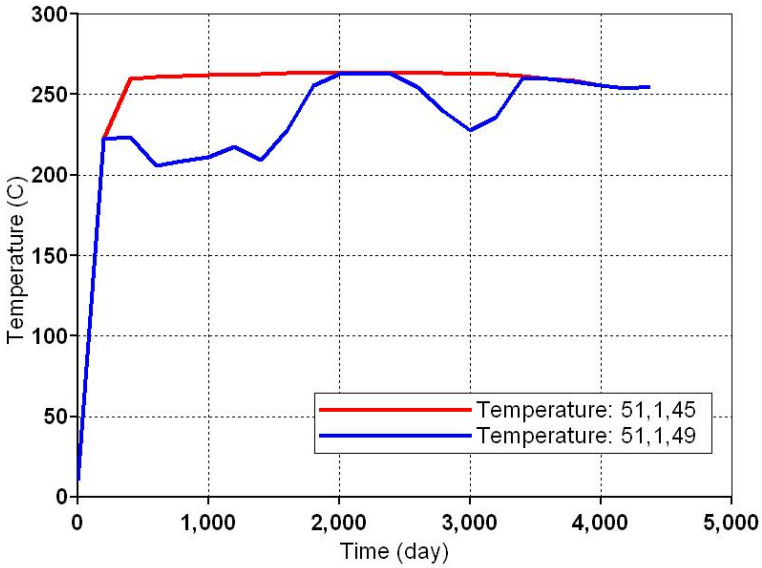


Figure 3.29: Well gridblock temperature, EnOpt of Example 2.

CHAPTER 4

# CONCLUSIONS

Production optimization of the SAGD operations was performed using the SPSA and EnOpt algorithms. The well control vector includes the CWE steam injection rate for the injector at each control step and bottomhole pressure for the producer at each control step. The control vector is adjusted to maximize the net present value (NPV). For a single horizontal injector/producer wellpair, SPSA and EnOpt are able to find controls that yield higher NPV than the base case and the subcool reactive control (steam trap).

The cSOR values obtained using the SPSA algorithm were lower than the EnOpt algorithm in both Example 1 and Example 2. However, having a low cSOR value did not result in higher NPV value in Example 1. This implies that cSOR may not be a good choice as the objective function for the production optimization, but NPV as the objective function can achieve both better thermal efficiency and higher cumulative oil production.

The base case without steam trap control using a constant steam injection rate and a constant production well bottomhole pressure results in an under-developed steam chamber and obtains a negative NPV. This is mainly due to live steam production caused by large pressure differential between the injector and producer without a liquid pool. The base case has a cumulative steam-oil ratio (cSOR) higher than 17.

The subcool reactive control maintains a constant temperature difference between the injected steam and the produced fluids and hence prevents live steam production. It yields realistic cSOR value below 4. However, the subcool reactive control only adjusts the production well bottomhole pressure to maintain a constant subcool

temperature. The given steam injection rate can be unrealistically high such that the injection well bottomhole pressure may fracture the reservoir and cause SAGD process failure.

The final controls obtained from SPSA and EnOpt follow similar behavior. The optimized SAGD process starts with a preheating period without any steam injection and during this period the heater option is turned on to heat oil around the wells. Following the preheating period is a period with an increasing injection rate. The injection rate decreases at late time when the steam chamber reaches caprock. The final production well bottomhole pressure controls increase at early time and maintain a plateau for a certain period of time and then it decreases. The behavior of final controls is consistent with that from the literature.

# BIBLIOGRAPHY


[1] Canadian oil sands. http://www.geoexpro.com/hydrocarbo/canadianoilsands/, May 2011.

[2] Recovery methods. http://www.heavyoilinfo.com/recovery-methods, May 2011.

[3] Worldwide heavy oil reserves by country. http://www.heavyoilinfo.com/blog-posts/worldwide-heavy-oil-reserves-by-country/, May 2011.

[4] A.M. Albahlani and T. Babadagli. A critical review of the status of SAGD: Where are we and what is next? In *Proceedings of SPE Western Regional and Pacific Section AAPG Joint Meeting*, number SPE 113283, March-April 2008.

[5] W. Bangerth, H. Klie, M.F. Wheeler, P.L. Stoffa, and M.K. Sen. On optimization algorithm for the reservoir oil well placement problem. *Computational Geosciences*, 10:303–319, 2006.

[6] X. Bao, Z. Chen, Y. Wei, C. Dong, J. Sun, H. Deng, and S. Yu. Numerical simulation and optimization of the SAGD process in Surmont oil sands lease. In *Proceedings of the Abu Dhabi International Exhibition & Conference*, number SPE 137579, November 2010.

[7] D.R. Brouwer and J.D. Jansen. Dynamic optimization of water flooding with smart wells using optimial control theory. *SPE Journal*, 9(4):391–402, 2004.

[8] D.R. Brouwer, G. Nævdal, J.D. Jansen, E.H. Vefring, and C.P.J.W. van Kruijsdijk. Improved reservoir management through optimal control and continuous model updating. In *Proceedings of the SPE Annual Technical Conference and Exhibition, Houston, Texas, 26-29 September*, number SPE 90149, 2004.

[9] R. M. Butler. SAGD comes of age! *The Journal of Canadian Petroleum Technology*, 37(7):9–11, July 1998.

[10] R.M. Butler. *Thermal Recovery of Oil and Bitumen*. Prentice-Hall, Inc, New Jersey, 1991.

[11] R.M. Butler. Steam-assisted gravity drainage: Concept, development, performance and future. *The Journal of Canadian Petroleum Technology*, 33(2):44–50, February 1994.

[12] R.M. Butler, G.S. McNab, and H.Y. Lo. Theorethical studies on the gravity drainage of heavy oil during in-situ steam heating. *The Canadian Journal of Chemical Engineering*, 59:455–460, August 1981.

[13] R.M. Butler and D.J. Stephens. The gravity drainage of steam-heated heavy oil to parallel horizontal wells. *The Journal of Canadian Petroleum Technology*, pages 90–96, April-June 1981.

[14] R.M. Butler and C.T. Yee. Progress in the in situ recovery of heavy oils and bitumen. *Journal of Canadian Petroleum Technology*, 41(1):31–40, January 2002.

[15] C.C. Card, N. Chakrabarty, and I. D. Gates. Automated global optimiztaion of commercial SAGD operations. In *Proceedings of the Petroleum Society's 7th Canadian International Petroleum Conference (57th Annual Technical meeting)*, number PAPER 2006-157, June 2006.

[16] C. Chen, G. Li, and A.C. Reynolds. Robust cosntrained optimization of short and long-term npv for closed-loop reservoir management. In *Proceedings of SPE Reservoir Simulation Symposium*, number SPE 141314, February 2011.

[17] Y. Chen and D.S. Oliver. Ensemble-based closed-loop applied to brugge field. In *Proceedings of the SPE Reservoir Simulation Symposium*, number SPE 118926, 2009.

[18] Y. Chen, D.S. Oliver, and D. Zhang. Efficient ensemble-based closed-loop production optimization. In *Proceedings of the SPE Improved Oil Recovery Symposium*, number SPE 112873, 2008.

[19] Y. Chen, D.S. Oliver, and D. Zhang. Efficient ensemble-based closed-loop production optimization. *SPE Journal*, pages 634–645, December 2009.

[20] S. Das. Improving the performance of SAGD. In *Proceedings of SPE International Thermal Operations and Heavy Oil Symposium*, number SPE/PS-CIM/CHOA 97921 PS2005-416, November 2005.

[21] N.R. Edmunds. Investigation of SAGD steam trp control in two and three dimensions. In *Proceedings of the SPE International Conference on Horizontal Well Technology*, number SPE 50413, March 1998.

[22] N.R. Edmunds. On the difficult birth of SAGD. *Journal of Canadian Petroleum Technology*, 38(1):14–17, January 1999.

[23] N.R. Edmunds. Investigation of SAGD steam trap control in two and three dimensions. *Journal of Canadian Petroleum Technology*, 39(1):30–40, January 2000.

[24] P. Egermann, G. Renard, and E. Delamaide. SAGD performance optimization through numerical simulations: Methodology and field case example. In *Proceedings of the SPE International Thermal Operations and Heavy Oil Symposium*, number SPE 69690, March 2001.

[25] G. Gao, G. Li, and A.C. Reynolds. A stochastic algorithm for automatic history matching. In *Proceedings of the SPE Annual Technical Conference and Exhibition*, number SPE 90065, 2004.

[26] G. Gao, G. Li, and A.C. Reynolds. A stochastic algorithm for automatic history matching. *SPE Journal*, 12(2):196–208, 2007.

[27] G. Gao and A.C. Reynolds. An improved implementation of the LBFGS algorithm for automatic history matching. *SPE Journal*, 11(1):5–17, 2006.

[28] I.D. Gates and N. Chakrabarty. Optimization of steam-assisted gravity drainage in mcmurray reservoir. In *Proceedings of the Petroleum Society's 6th Canadian International Petroleum Conference (56th Annual Technical meeting)*, number PAPER 2005-193, June 2005.

[29] I.D. Gates, J. Kenny, I.L. Hernandez, and G.L. Bunio. Steam-injection strategy and energetics of steam-assisted gravity drainage. *SPE Reservoir Evaluation & Engineering*, 10(1):19–34, February 2007.

[30] I.D. Gates and C. Leskiw. Impact of steam trap control on performance of steam-assisted gravity drainage. *Journal of Petroleum Science and Engineering*, 75:215–222, 2010.

[31] Y. Ito and S. Suzuki. Numerical simulation of the SAGD process in the hanging-stone oil sands reservoir. *Journal of Canadian Petroleum Technology*, 38(9):27–35, January 1999.

[32] X. Jia, L.B. Cunha, and C.V. Deutsch. Investigation of stochastic optimization method for automatic history matching of SAGD processes. *Journal of Canadian Petroleum Technology*, 48(1):14–18, January 2009.

[33] J. Kiefer and J. Wolfowitz. Stochastic estimation of a regression function. *Ann. Math. Statist.*, 23:462–466, 1952.

[34] D.P. Komery, R.W. Luhning, and J.C. O'Rourke. Towards commercialization of the UTF project using surface drilled horizontal SAGD wells. *Journal of Canadian Petroleum Technology*, 38(9):36–43, September 1999.

[35] J.F.B.M. Kraaijevanger, P.J.P. Egberts, J.R. Valstar, and H.W. Buurman. Optimal waterflood design using the adjoint method. In *Proceedings of the SPE Reservoir Simulation Symposium*, number SPE 105764, page 15, 2007.

[36] G. Li and A.C. Reynolds. Uncertainty quantification of reservoir performance predictions using a stochastic optimization algorithm. *Computational Geosciences*, 15(3):451462, 2011.

[37] R.J. Lorentzen, A.M. Berg, G. Nævdal, and E.H. Vefring. A new approach for dynamic optimization of waterflooding problems. In *Proceedings of the SPE Intelligent Energy Conference and Exhibition*, number SPE 99690, 2006.

[38] H.A. Mendoza, J.J. Finol, and R.M. Butler. SAGD, pilot test in Venezuela. In *Proceedings of SPE Latin American and Caribbean Pertoleum Engineering Conferemce*, number SPE 53687, April 1999.

[39] T.N. Nasr and O.R. Ayodele. Thermal techniques for the recovery of heavy oil and bitumen. In *Proceedings of SPE International Improved Oil Recovery Conference*, number SPE 97488, December 2005.

[40] J. Nocedal and S.J. Wright. *Numerical Optimization*. Springer, New York, 2006.

[41] J. Nwaozo. Dynamic optimization of a water flood reservoir. Master's thesis, University of Oklahoma, Norman, Oklahoma, 2006.

[42] G. Parmar, L. Zhao, and J. Graham. Start-up of SAGD wells: History match, wellbore design and operation. *Journal of Canadian Petroleum Technology*, 48(1):42–48, January 2009.

[43] N.V. Queipo, J.V. Goicochea, and S. Pintos. Surrogate modeling-based optimization of SAGD processes. In *Procedings of SPE International Thermal Operations and Heavy Oil Symposium*, number SPE 69704, March 2001.

[44] A.C. Reynolds, M. Zafari, and G. Li. Iterative forms of the ensemble Kalman filter. *Proceedings of 10th European Conference on the Mathematics of Oil Recovery*, 2006.

[45] M. Saltuklaroglu, G.N. Wright, P.R. Conrad, J.R. McIntyre, and G.J. Manchester. Mobil's SAGD experience at Celtic, Saskatchewan. *Journal of Canadian Petroleum Technology*, 39(4):45–51, April 2000.

[46] P. Sarma, L.J. Durlofsky, and K. Aziz. Efficient closed-loop production optimization under unceratinty. In *Proceedings of the SPE/EAGE Annual Conference*, number SPE 94241, 2005.

[47] P. Sarma, L.J. Durlofsky, and K. Aziz. Implementation of adjoint solution for optimal control of smart wells. In *Proceedings of the SPE Reservoir Simulation Symposium*, number SPE 92864, 2005.

[48] H. Shin and M. Polikar. Optimizing the SAGD process in three major Canadian oil-sands areas. In *Proceedings of SPE Annual Technical Conference and Exhibition*, number SPE 95754, October 2005.

[49] J.C. Spall. Multivariate stochastic approximation using a simulataneous perturbation gradient approximation. *IEEE Transactions Automat. Control.*, 37(3):332–341, 1992.

[50] J.C. Spall. An overview of the simultaneous perturbation method for efficient optimization. *John Hopkins APL Technical Digest*, 19(4):482–492, 1998.

[51] J.C. Spall. Adaptive stochastic approximation by the simultaneous perturbation method. *IEEE Transactions on Automatic Control*, 45(10):1839–1853, 2000.

[52] C. Wang, G. Li, and A.C. Reynolds. Production optimization in closed-loop reservoir management. *SPE Journal*, page 506, September 2009.

[53] H.Y. Wang. Application of temperature observation wells during sagd opeartions in a medium deep bitumen reservoir. *Journal of Canadian Petroleum Technology*, 48(11):11–15, November 2009.

[54] C. Yang, C. Card, and L. Nghiem. Economic optimization and uncertainty assestment of commercial SAGD operations. *Journal of Canadian Petroleum Technology*, 48(9):33–40, September 2009.

[55] C. Yang, C. Card, L. Nghiem, and E. Fedutenko. Robust optimization of SAGD operations under geological uncertainties. In *Proceedings of SPE Reservoir Simulation Symposium*, number SPE 141676, February 2011.

[56] H. Zhao, C. Chen, S. Do, G. Li, and A.C. Reynolds. Maximization of a dynamic quadratic interpolation model for production optimization. In *Proccedings of the SPE Reservoir Simulation Symposium, The Woodlands, Texas, USA, 21-23 February*, number SPE 141317, 2011.